Ammonia combustion on a swirl and bluff body stabilized burner

Miguel Alexandre Coelho Franco

Thesis to obtain the Master of Science Degree in

Mechanical Engineering

Supervisors: Prof. Miguel Abreu de Almeida Mendes

Eng. Rodolfo Cavaliere da Rocha

Examination Committee

Chairperson: Prof. José Manuel da Silva Chaves Ribeiro Pereira

Supervisor: Prof. Miguel Abreu de Almeida Mendes

Member of the Committee: Prof. Pedro Jorge Martins Coelho

January 2021

Acknowledgements

In the first place I would like to thank to all the IDMEC combustion laboratory personnel for letting me work with them and for all the scientific and non-scientific discussions, which make me feel welcome and in a good environment for working.

I would like to give an individualized thank to Rodolfo, for all the help he gave both in experiments and in scientific analysis of the results and to Mr. Manuel Pratas, for all the work done by him in the laboratory, assisting and making everything running correctly during the experiments. Also, I would like to thank Professor Miguel Mendes for receiving me during a difficult time and helping and pushing me to finish this work.

Finally, I would like to give a special thanks to Professor Mário Costa, who was the mind behind the idealization of this work. I would like to thank him for everything he taught me, every scientific discussion we had and every experiences he provided me.

Resumo

Amónia (NH_3) tornou-se uma promissora alternativa aos combustíveis fósseis, no entanto, a sua combustão apresenta alguns desafios com a sua baixa velocidade de chama, baixa temperatura e altas emissões de NO_x, sendo necessários novos sistemas que ultrapassem estas dificuldades. Neste trabalho foi projetado um novo queimador para a combustão de NH_3, combinando técnicas de "swirl" e recirculação através de um "bluff-body", e o mesmo foi testado com chamas de NH_3/H_2/ar. Foram obtidos diagramas de estabilidade para 3 potências diferentes de modo a descobrir os limites operacionais do queimador. De seguida, foram medidas, na exaustão, as emissões de NO_x e de NH_3 para 1.9 kW e para diferentes razões de equivalência (ϕ) e diferentes frações molar de NH_3 no combustível (x_{NH_3}), bem como medidas de temperatura, concentrações de NO_x e de O_2 dentro do tubo de quartzo. Foi obtida boa estabilidade com uma gama de operacionalidade relativamente larga, aumentando com a potência, incluindo para chamas de amónia pura, obtidas apenas para 1.9 kW. As temperaturas e as concentrações de NO_x foram maiores na zona de recirculação. As concentrações de NO_x aumentaram com o ϕ e aumentaram com a diminuição de χ_{NH_3}. As concentrações também diminuíram ao longo do eixo, onde se pensa que esteja a ocorrer "selective non-catalytic reduction" (SNCR). Globalmente, o queimador funcionou bem como esperado, produzindo uma vasta gama de resultados. Além disso, com este trabalho abrem-se perspetivas para o uso deste design de queimador para futuro uso em turbinas a gás.

Palavras chave: Combustão de amónia, queimador com swirl, estabilização de chama por bluff-body, caracterização experimental, concentrações de NO_x, queimador à escala laboratorial.

Abstract

Ammonia (NH_3) is a promising alternative to fossil fuels, however, its combustion presents challenges such as low flame speed, low temperature and high NO_x emissions. Therefore, new systems are required to overcome these difficulties. In this work, a new burner for NH_3 combustion was designed, combining swirl and bluff-body recirculation, and tested for NH_3/H_2/air flames. Stability diagrams were obtained for 3 different thermal inputs to assess the operational range of the burner. Afterwards, NO_x and NH_3 exhaust emissions were measured for 1.9 kW and for different equivalence ratios (ϕ) and NH_3 molar fractions in the fuel (x_{NH_3}), as well as measurements of temperatures, NO_x and O_2 concentrations throughout the inside of the combustor. Good stability with relatively wide operational ranges were verified, increasing with the thermal input, including for pure ammonia/air flames, achieved only for 1.9 kW. Temperatures and NO_x concentrations were higher in the recirculation zone. NO_x concentrations increased with the increase of ϕ and with the decrease of x_{NH_3} . Also, NO_x concentrations decreased along the combustor axis, where selective non-catalytic reduction (SNCR) is believed to occur. Globally, the burner presented good operational characteristics, producing a wide range of data. Moreover, this work opens perspectives on the use of this burner design in future ammonia gas turbines.

Keywords: Ammonia combustion, Swirl burner, Bluff-body flame stabilization; Experimental characterization, NO_x concentrations, Laboratory-scale burner.

Table of contents

List of figures

List of tables

Nomenclature

A/D converter – Analog to digital converter

CFR – Cooperative Fuel Research

CI engines – Compression Ignition engines

CIT – Combustion Inlet Temperature

CR – Compression Ratio

EI_{NO_x} – NO_x emission index

GHG – Green House Gases

HGS – Hydrogen Generation System

HPCR – High Pressure Combustion Rig

ICE – Internal Combustion Engine

IEA – International Energy Agency

LHV -Low Heating Value

ppm – parts per million

PSR – Perfectly Stirred Reactor

SCR – Selective Catalytic Reduction

SI engine – Spark Ignition engine

SNCR – Selective Non-Catalytic Reduction

TPES – Total Primary Energy Supply

V_{coflow} – velocity of the air co-flow injection

V_{fuel} – velocity of the fuel injection

V_{H_2} – volume of injected hydrogen

V_{NH_3} – volumes of injected ammonia

ϕ – equivalence ratio

x_{NH_3} – NH_3 molar fraction

1 Introduction

1.1. Motivation

Nowadays, energy, in its many ways, drives almost everything in our society, from electricity production to vehicles motion, from food production to cooking, etc. Along with the global population increase, we can observe an increase of energy demand. This tendency can be corroborated by looking at data from the International Energy Agency (IEA) about Total Primary Energy Supply (TPES) in the last few years.

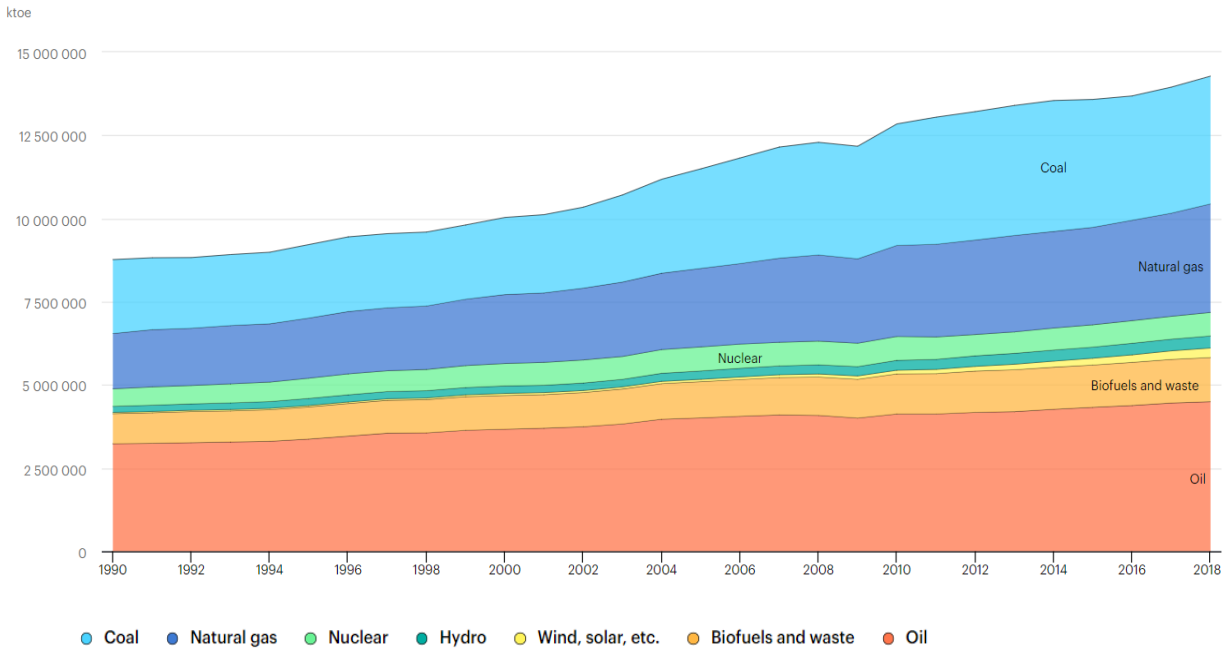

Figure 1.1 - World total energy supply by source between 1990 and 2018 [1]

Figure 1.1 shows the growing need for energy with the great dependence on fossil fuels (coal, natural and oil, for example) for this purpose. In fact, data from the same source shows that about 64% of the electricity production comes from the combustion of these fuels (Figure 1.2).

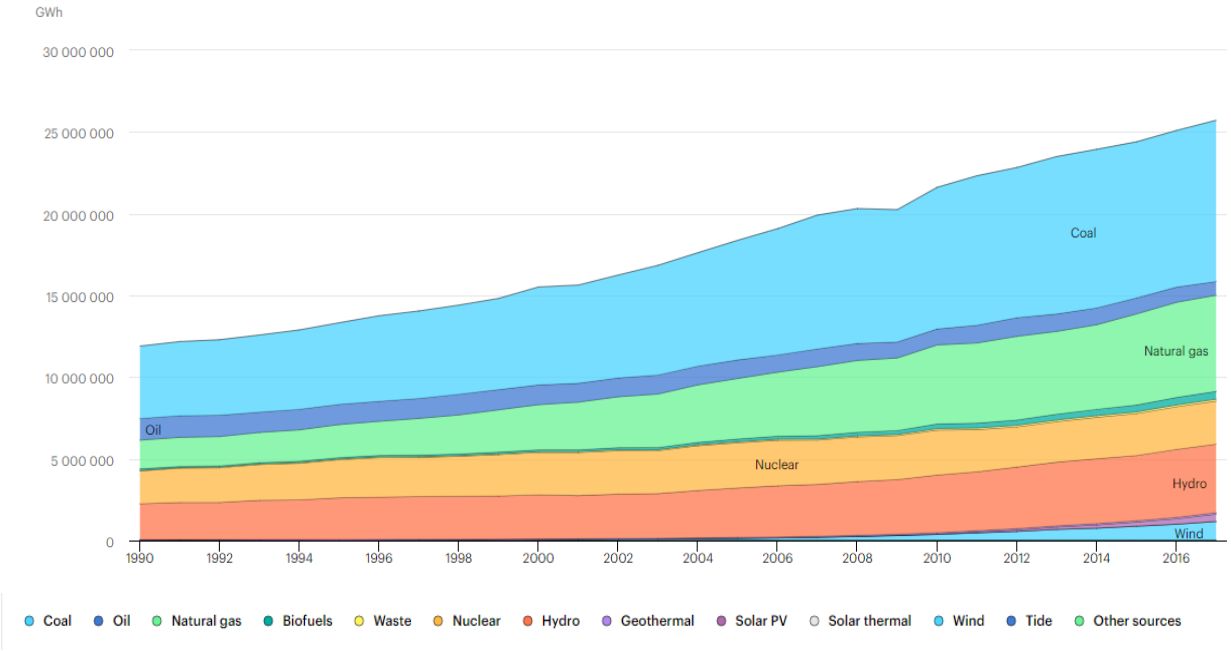

Figure 1.2 - World electricity generation by source between 1990 and 2018 [1]

With the burning of fossil fuels, it comes one of the most concerning problems discussed between our society, global warming. The combustion of fossil fuels generates some concerning exhaust gases, usually known as greenhouse gases (GHG), that can be harmful for the environment and for living species, mainly because of their carbon content. This generation of GHG is well documented and consists of a big problem in the processes of combustion of fossil fuels.

Renewable energy sources like solar energy, wind energy, hydro power or geothermal energy are good ways to substitute the fossil-based power generation. However, these kinds of sources are not constant in time and are not available in every country, which by themselves could not be enough to supply all the power needed.

Despite the decrease of the tendency to burn fossil fuels, it is expected that combustion continues to be the primary source of energy conversion. Following this fact, the scientific community has been doing massive research to provide new alternative fuels to power generation.

Throughout the different possibilities, hydrogen was one of the most promising alternative fuels specially because of its carbon free content, which lead to no GHG emissions. On the other hand, the interest of this fuel is diminished by its difficulty of transportation and storage. Hydrogen requires very low temperature to be liquified and very high pressure to be stored at room temperature (Table 1.1), which makes it dangerous and expensive to transport and store.

Table 1.1 – Thermal properties and combustion characteristics of ammonia, hydrogen and other hydrocarbon fuels [2]

Fuel	NH_3	H_2	CH_4	C_3H_8
Boiling temperatureat 1 atm (°C)	−33.4	−253	−161	−42.1
Condensation pressure at 25 °C (atm)	9.90	N/A	N/A	9.40
Lower heating value, LHV (MJ/kg)	18.6	120	50.0	46.4
Flammability limit (Equivalence ratio)	0.63∼1.40	0.10∼7.1	0.50∼1.7	0.51∼2.5
Adiabatic flame temperature (°C)	1800	2110	1950	2000
Maximum laminar burning velocity (m/s)	0.07	2.91	0.37	0.43
Minimum auto ignition temperature (°C)	650	520	630	450

It is in this context that ammonia starts to be regarded as another possible alternative carbon free fuel. Ammonia, which started to be considered as a hydrogen carrier, rapidly started to be used as a direct fuel. It is been used and produced for more than 100 years and, besides the possibility of being a fuel, it has been used as a fertilizer, as a refrigerant for industrial cooler and even as essential compound on selective catalytic reduction (SCR) or selective non-catalytic reduction (SNCR) in most of the thermal power stations. All these facts mean that ammonia production, transportation and storage are well established and in fact, many power plants have already ammonia storage tanks installed. Moreover, looking at Table 1.1 both boiling temperature and condensation pressure of NH_3 are very similar to those of propane (C_3H_8), which could mean that the structures already existent for transportation and storage of propane could be used for ammonia with none or few modifications.

But not only through combustion it can be generated power from ammonia. It can be used in fuel cells [3] and like has been said before, ammonia started as a chemical storage for H_2 [4], where the hydrogen based fuel cells are fed with NH_3 and then crack it to produce H_2. However, due to ammonia's well established production, handling and utilization, it started to be regarded as a direct fuel for fuel cells [5].

Ammonia production is based on the combination of hydrogen and nitrogen (N_2). While the N_2 comes from the air, the hydrogen used comes essential from natural gas reformation, which although ammonia burning will produce no CO_2 emissions, its production involves the emission of this pollutant. However, it is being developed more and more ways to produce the so-called "green ammonia" using hydrogen produced by renewable sources, for example the water electrolysis by renewable energies.

With the production issue surpassed, ammonia still has its drawbacks, namely the narrow flammability range, low flame speed, high ignition delay time, high NO_x emissions, etc. Having these difficulties in mind, innumerous researches and investigations have been done all over the past years to suppress and overcome these difficulties and improve and make possible the combustion of ammonia in gas turbines, internal combustion engines, etc.

1.2. Literature review

As already mentioned, ammonia is starting to be an attractive alternative fuel to fossil fuels and being the focus of many different investigation works. Despite the recent growing interest in this subject, it can be rewind to the 2nd world war to see some practical work with ammonia combustion.

In 1945, Korch [6] published a report of the work done by him and his co-workers during the 2nd World War in Belgium regarding the use of ammonia for fuelling motor buses. It all started when, in 1942, the supply of diesel for buses was interrupted because of the war. Specialists quickly realized that there was not enough quantity of liquid petroleum gas for running the buses and the compressed coal gas has low energy density which would require large fuel containers. Due to all of this, the author was approached to find a solution using ammonia for the motor buses, which he considered a good motor fuel due to the less air requirement for combustion, its expansion through combustion and, the possibility of ammonia to be used with high compression ratios. However, the author recognized the difficulty of ammonia to burn by itself, so he adopted a mixture between compressed coal gas and ammonia as fuel. The buses worked for months with this mixture, and after thousands of miles, the author recorded, when comparing the mixture with gas-oil, no power losses, no increase of lubrification-oil consumption and, contrary to expectations, there was no corrosion on the motors. This work was probably one of the first of its kind and gave good perspectives for the use of NH3 as fuel.

After that, the interest of ammonia for fuelling slightly aroused in the next few years. In 1967 Pratt [7] did experimental tests to investigate scaling and combustion of gaseous ammonia in gas turbine combustor. He concluded that the principal problem of using ammonia in gas turbines is the slow chemical reaction with air and poor mixing which decrease the combustion efficiency. Apart from cracking, the author appointed some solutions for improving flame stability such as the use of smaller fuel nozzle orifices, to increase velocity and the use of 2 or more combustors in parallel instead of just one.

In the same year, Starkman and Samuelsen [8], recognising the difficulty of ammonia to be ignited, performed tests in a standard CFR engine to investigate the combustion characteristics of ammonia. The results proved that slow flame speed is the main obstacle for successfully burning this fuel. They noticed that decomposition of ammonia prior ignition is the most important variable to accomplish a successful combustion. It was also observed that the values of NO at the exhaust were higher than the predicted and these values couldn't come just from the equilibrium. It was concluded that these results are a result from ammonia incomplete conversion.

Also in 1967, Verkamp et al. [9] conducted studies to characterize some features of ammonia combustion in gas turbines. The authors found that the minimum ignition energy of ammonia is considerably higher than hydrocarbon fuels and the range of equivalence ratios for stable flame was much narrower. These findings helped them to conclude that NH_3 wasn't a good substitute fuel for conventional gas turbines unless ammonia is injected in a gaseous state and the energy of the ignition

system is increased. The authors tried 2 techniques to improve the combustion properties. The first was the use of additives in concentrations of 5% by volume, which gave no results on the improvement of flame stability. The second one was the partial pre-dissociation of ammonia before injection, where they found that 28% dissociated NH_3 has similar properties as methane that in turn could be used as hydrocarbon fuel substitute in gas turbine systems.

These works set the basis for the progress of the work to be done when dealing with ammonia combustion. However, its continuation took a brief break most likely because of the problems appointed by the previous authors regarding the difficulty of burning ammonia.

However, the combustion of ammonia gained a new interest in the last 20 years since there was a need of the scientific community for more alternative “clean fuels” to reduce pollution and comply with the regulations imposed on the countries. With that being said, many experiments and reports are being done and published after the beginning of the century giving insights of the usage of ammonia combustion throughout many different technologies and the techniques used to surpass the difficulties found and well known since the first works. The first approaches were naturally trying to burn ammonia blended with other fuels with old technologies used for other fuels with none or little changes.

In 2008, Reiter and Kong [10] thought that the literature of ammonia combustion in engines was still limited and decided to do some experiments to demonstrate the feasibility of using ammonia in compression-ignition (CI) engines. They used a multi-cylinder, turbocharged diesel engine with a dual-fuel approach (diesel-NH3) needing only a slight modification on the intake system to supply ammonia, while keeping the diesel injection system unchanged. The tests were carried for various combinations of diesel-ammonia fuel blends, and at various engine speeds and loads. It was found that for the same engine torque, it can be used a replacement by ammonia of 95% (by volume). For 40-80% of the total energy being provided by ammonia there was a reasonable fuel economy and NO_x emissions are reduced when the replacement doesn’t exceed 60%. CO_2 emissions decreased with the ammonia introduction being nearly proportional to the ammonia replacement. The authors also used biodiesel instead of diesel in the dual fuel approach tests drawing similar results of those of diesel and concluded about the possibility of successfully using ammonia for fuelling CI engines.

Reiter and Kong [11] continued their tests on this engine and in 2011, they came with new data regarding its operation in terms of emissions. For constant engine power operation, beside the results found in the previous work [10] for NOx emissions, they found that CO and HC emissions were generally higher when compared with only diesel fuel (Figure 1.3 (a)-(c)) due to the lower combustion temperatures which may lead to incomplete combustion. It was also observed that soot emissions decreased with the increase of ammonia replacement, because of the less diesel supply. Despite the overall relatively high ammonia combustion efficiency, exhaust ammonia emissions were measured between 1000-3000 ppm (Figure 1.3 (d)). These values are higher than the regulated values, being dangerous for human health, leading the authors to complement their previous conclusions that using NH3 on CI engines is possible,

however different injection strategies need to be tested and exhaust gas after-treatment needs to be used.

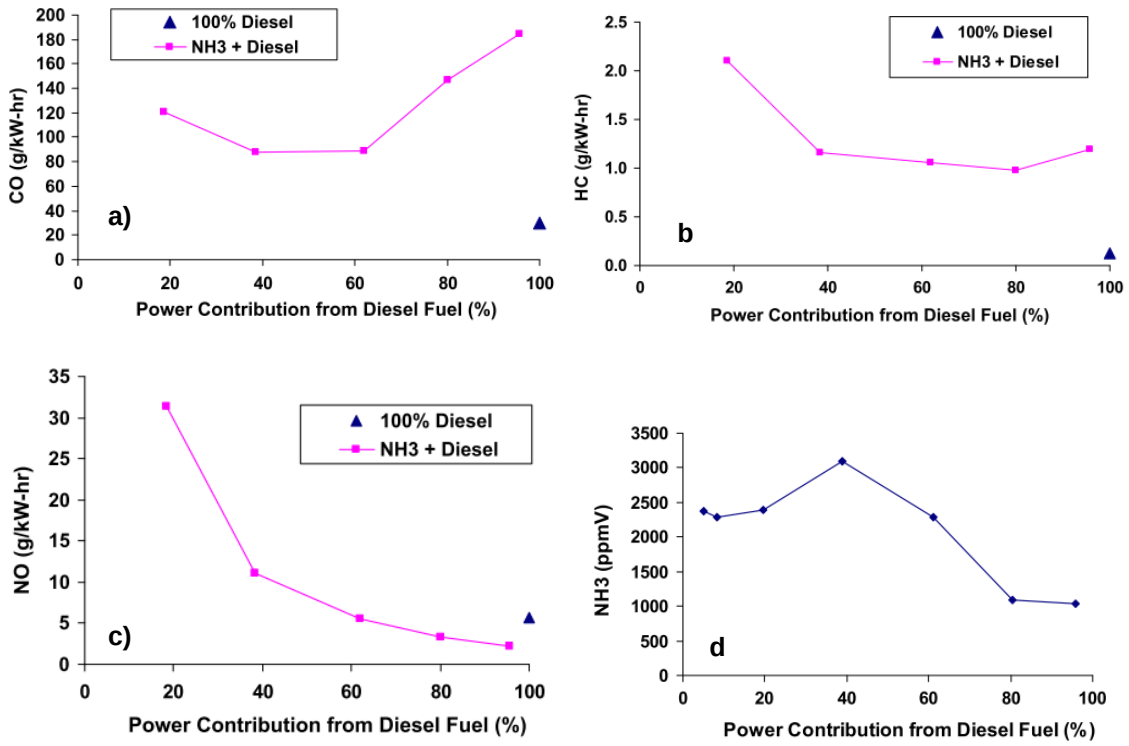

Figure 1.3 – Emissions under constant power output using different combinations of ammonia/diesel in the fuel. Adapted from [11]

Later in 2012, S.S. Gill et al. [12] performed tests to investigate the best dual fuel approach to supply CI engines between pure H_2, pure NH_3 and partially dissociated NH_3 in addition to diesel. In general, pure NH_3 increased fuel consumption while the other 2 options slightly decreased it and all of them reduced the CO_2 emissions. The use of pure NH_3 performed better than dissociated NH_3 in terms of stability, increasing the HC emissions due to the lower temperature and increasing the overall NO_x emissions and N_2O formation. The H_2 addition looks the most promising solution in terms of engine and emission performances, only increasing NO_x emissions due to higher temperatures. However, pure H_2 coming from NH_3 requires sophisticated technologies making it not practical on-board a vehicle. The authors then conclude that partially dissociated NH_3 is the best option to the use of ammonia in CI engines since it has similar emissions as pure H_2, having lower NH_3 and N_2O emission compared to pure NH_3.

But not only blends of ammonia and diesel were tried on CI-engines. C.W. Gross and S.C. Kong [13] performed experiments to evaluate combustion and emission characteristics of burning blends of ammonia and dimethyl ether (DME) in a compression-ignition engine, with the main goal of reducing exhaust ammonia emissions. The original fuel injection system was replaced for a new one, to make possible liquid injection. Double injection was also tested to see if it had improvements. The results showed that the use of Ammonia in the fuel increases the ignition delay time, due to its high autoignition temperature and low flame speed. The soot emissions remain low while CO and HC emissions increase,

mainly due to the decrease of combustion temperature. The NOx emissions increase when ammonia is used, due to fuel NO_x formation, while the exhaust ammonia emissions are reduced with the new injection strategy, being the values on the order of hundred ppm. The authors observed that increasing the injection pressure led to improved combustion characteristics and emissions, allowing the use of higher NH_3 content mixtures. Additionally, they noticed that the use of double injection, in the overall did not change the operating range but in some operating conditions it can improve combustion. The author agreed that more development in ammonia engine technology will increase the potential of ammonia as fuel.

Ryu et al. [14] also did experiments on a diesel compression-ignition engine with blends of ammonia and DME. Appropriate injection strategies were developed, and 3 mixtures were used, 100% DME, 60%DME-40%NH_3 and 40%DME-60%NH_3. In terms of engine performance, both engine speed and power showed limitations, relative to 100% DME, with the increase of ammonia concentration in fuel. Also, injection time needed to be increased with the increase of NH_3 due to its resistance to autoignition. In terms of emissions, CO and HC are high due to low combustion temperature, which results in incomplete combustion. NH_3 emissions increase with the increase of NH_3 in the fuel mixture, reaching unacceptable values, and NO_x increases due to the formation of fuel NO_x. Despite soot emissions increases slightly due to incomplete combustion when using higher content of NH_3, it remains extremely low. The authors conclude that high concentration of ammonia can be used in CI diesel engines with appropriate injection techniques requiring exhaust after-treatment for reducing gaseous emissions.

In parallel to CI engines investigations with ammonia, some researchers were doing similar experiments in spark-ignited (SI) engines. Morch et al. [15] did some basic experiments to obtain preliminary data of ammonia/hydrogen mixtures combination using a CFR SI-engine. The tests consisted of varying the fuel mixture, the excess air ratio and the compression ratio (CR) to evaluate the performance and efficiency of the engine. The authors found that 10 vol% of hydrogen content in the fuel gives the best efficiency and, due to the capability of use a high CR, these mixtures have higher efficiency and power when compared with gasoline at its maximum possible CR. They also measured NO_x emission and concluded that, despite the mechanisms of NO_x formation are different, the values of NO_x emitted by these mixtures are similar to the ones of gasoline. These results support the possibility of using ammonia/hydrogen mixtures as fuel for SI engines, however the authors still recognize the need for more investigations and improvements such as the use of higher engine speeds and SCR for NO_x reduction.

To evaluate the potential of ammonia substitution to improve safety of hydrogen use as fuel, S. H. Lee et al. [16] performed tests on a spark-ignited spherical laminar premixed flame burner. They varied both ammonia substitution level in NH_3/H_2 fuel mixture and equivalence ratio to assess performance aspects such as laminar burning velocity, flame front instabilities and NO_x and N_2O emissions. It was observed that ammonia substitution can suppress some instabilities of hydrogen/air flames, particularly for lean conditions, which does not happen with methane substitution. Moreover, they observed that ammonia substitution reduces temperatures and laminar burning velocity with higher decrease for rich conditions.

The authors also recorded that NO_x and N_2O emissions increase with the NH_3 substitution, but the amount of increasing is lower for rich conditions.

The scientific community began to see the benefits of burning hydrogen/ammonia mixtures, not only because of the “carbon free” content of those mixtures but also because of the improvement in safety when compared with pure hydrogen. With that being said, the next natural step was trying to create these mixtures supplying only NH_3. Due to its high content of hydrogen, cracking the NH_3 before ignition will produce the H_2/NH_3 mixtures desired without the need of supplying pure H_2 overcoming all the difficulties associated to it.

K. Ryu et al. [17], investigate the effects of using ammonia dissociation into hydrogen, by means of a catalyst, on engine performance, combustion characteristics and exhaust emission in a SI engine fuelled by ammonia and gasoline. In general, it was found that the use of the catalyst improved the combustion and engine performance and reduced exhaust emissions (CO, HC, NH_3 and NO_x). However, the authors especially noticed that for low loads, i.e. low NH_3 flow rate, the experiments using the catalyst showed better results. The engine power increased while the fuel consumption decreased because of the higher conversion rate resulting from the higher residence time inside the catalyst caused by the low flow rate of NH_3. These results demonstrated the feasibility of using ammonia as a hydrogen carrier for fuelling internal combustion engines towards a clean combustion system.

Sensibly at the same period Frigo and Comotti [18], despite the previous experiment [17], reported their work where they claimed to be the first time that an SI engine operated with a mixture of ammonia and hydrogen, being the latest produced from ammonia cracking on a catalytic reactor. This experiment followed their previous work [19] and the intention is to use the ICE fuelled by NH_3-H_2 mixture to recharge batteries in an electric vehicle. For that the authors used a hydrogen generation system (HGS) with a cracking reactor housing a ruthenium-based catalyst, coupled with a twin cylinder SI engine. The main goal was to access the viability of ammonia dissociation before the engine supply. In this study it was used a higher hydrogen flow rate than the minimum required for engine operation, which improved efficiency, fuel economy and engine cyclic variability, but simultaneously increase NO_x emission. However, the NO_x emissions are still close to those of gasoline and are not considered a huge problem by the authors since they can be reduced by a catalyst or in case of higher emissions (lean mixtures) by using SCR systems, with the advantage of ammonia being already available in the system. In general, the authors found efficiencies using NH_3-H_2 mixtures similar to those of gasoline and reported no considerable ammonia emission in exhaust gases. With all the stated results, the authors proved it was possible to successfully run an engine with NH_3-H_2 mixtures using only ammonia as principal a fuel, obtaining the hydrogen from it.

After so many different experiments the researchers arrived to a point where they shifted their way of thinking and tried to make different approaches. Instead of trying to use old technologies to burn ammonia, they started to investigate better ways to do it towards creation of a new combustor for the purpose.

One of the first steps was to abandon the premixed injection, where the fuel and the air were mixed before injection and try different strategies to evaluate the benefits. In 2013, D. H. Um et al. [20] provided an experimental database for modelling non-premixed NH_3-H_2-air flames. They conducted tests in a non-premixed co-flow type burner to evaluate the effects of partially NH_3 substitution on stability limits and NOx emissions and the effect of air co-flow and fuel injection velocities (V_{coflow} and V_{fuel}). The results showed that there was a significant reduction in stability limits with the NH_3 substitution and that for a given V_{coflow} / V_{fuel} ratio, the flame length increases with the NH_3 substitution. Concerning the NOx emissions, this group noticed that NOx emission index (EI_{NO_x}), that they defined as the fraction of the mass of the produced NOx per mass of provided fuel (NH_3+H_2), doesn't increase in big proportion with the increase of NH_3. Also, they observed that EI_{NO_x} decreases with the increase of air (V_{coflow}) and that it decreases and then increases with increasing of fuel (V_{fuel}) (Figure 1.4). These findings helped to conclude the potential of NH_2 substitution as a green additive for improving the safety of H_2 use, with reasonable levels of NOx emissions, with non-premixed flames.

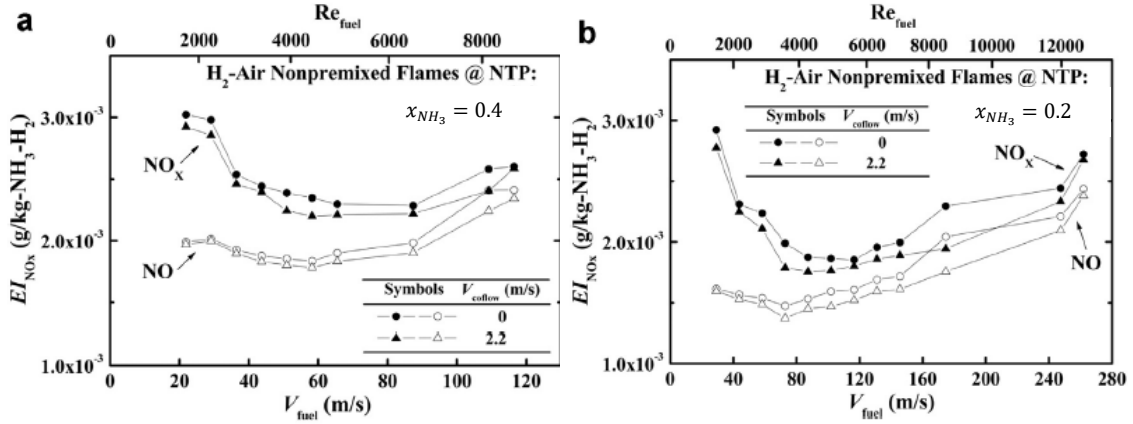

Figure 1.4 – Effects of x_{NH_3}, V_{coflow}, V_{fuel} on NO_x emissions. V_{coflow} = 0 and 2.2 m/s, V_{fuel} = 21.8 to 262 m/s and x_{NH_3}= 0.4 (a) and 0.2 (b). Adapted from [20].

After this experiment, swirl combustors were started to be used in an attempt to improve stability and combustion performance of NH_3 with the ultimate goal of burning 100% of ammonia. In 2015, A. Valera-Medina et al. [21] did experiments in a high-pressure combustion rig (HPCR) with a generic lean-premixed swirl burner to assess the stability and emissions of ammonia blended both with methane and hydrogen. They reported their trials of attempting to reach 100% NH_3 combustion, but they found only possible until 80% when blended with CH_4 and found that 50% NH_3 blended with H_2 has similar burning velocity as methane. The results showed that in NH_3-CH_4 blends for lean conditions ($\phi \approx 0.7$) there is high NO_x and low CO, while when reaching rich conditions (ϕ=1.1) NOx decreased but CO increased considerably. The NH_3-H_2 blend showed a narrow stability range with high NO_x emission for the highest equivalence ratio (ϕ=0.577). The main conclusion is that high stability, low emissions and high temperature can be achieved with these blends but only for a small interval of equivalence ratios.

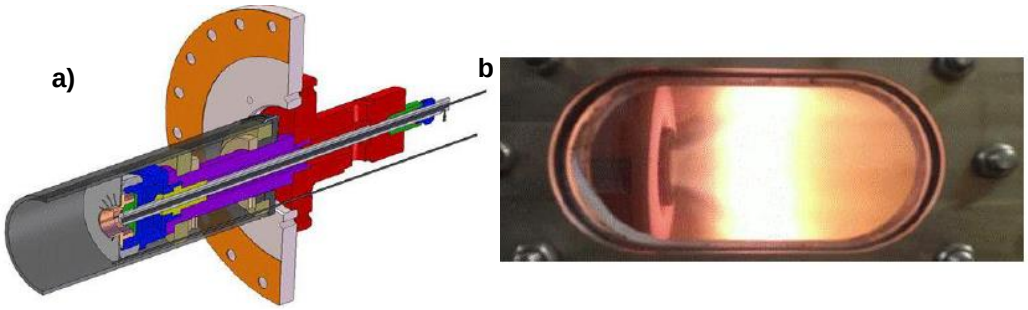

Figure 1.5 – Schematic of the generic swirl burner used by Valera-Medina's group (a) and a NH_3/CH_4/air swirl flame (b) Adapted from [21].

After their first trials on ammonia combustion on swirl burners, the group of Agustin Valera-Medina did a numerical and experimental work [22] on ammonia-methane blends using the same premixed generic swirl burner [21] to evaluate flame stability and emissions, for different equivalence ratios and fuel mixture content, providing some insights on ammonia blends combustion. They made their experiments under atmospheric pressure and medium pressurized conditions. It was found that only for a mixture of 60% NH_3 and CH_4 the tests were feasible, being mixtures with more content of NH_3 either impossible to ignite or unstable. The results showed that the lowest total emissions were obtained for an equivalence ratio between 1.15 and 1.25, but still with high values of CO, and that increasing of pressure could improve combustion and give lower emission (Figure 1.6). When comparing numerical and experimental results, they observed that the models used over-estimate CO values and under-predict NO_x values, which means that these models still need improvements for ammonia combustion. They also noticed that medium/high swirl numbers can produce some instabilities where they conclude that fully premixed combustion is not the most effective injection strategy for burning this blend and that a lower swirl number should be used, ensuring that the vortex breakdown phenomenon still occurs.

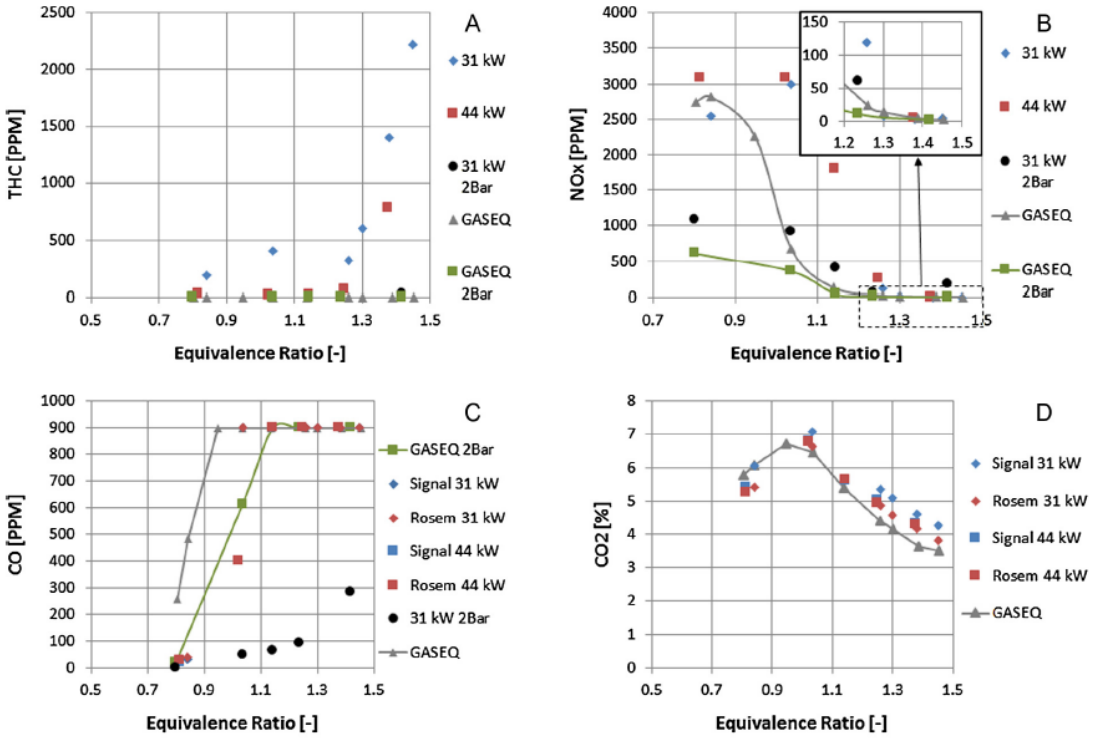

Figure 1.6 – Emissions experimental measurements and predictions. Adapted from [22].

The same authors, in 2017 [23] continued their studies but this time, performing numerical and experimental tests for a 50:50 (vol.%) mixture of ammonia and hydrogen for lean premixed combustion in a generic swirl combustor, used in the previous works [21], [22]. With their operation conditions, they found the flame stable for equivalence ratios between 0.43 and 0.52 ($0.43<\phi<0.52$), for a thermal input of 31 kW. Despite the flame velocity of this mixture can be similar to methane, the narrow range of stability is caused by the high diffusivity and reactivity of hydrogen, causing flashback, and also due to the high swirl number. They also still registered high values of NO_x mainly because of the high production of OH and O radicals. However, the authors concluded that their species production shows promising data for creating a novel combustion system with lower swirl number and flue gas recirculation for further NO_x reduction.

Following their previous work [23] and to improve NH_3 combustion, giving more data of its influencing factors, in 2019, experimental and numerical tests were undertaken by Valera Medina et al. [24] to give initial data on the use of 70% NH_3 – 30% H_2 fuel blend in gas turbine environment. They used a generic swirl burner with around 40kW output power under atmospheric pressure for rich conditions ($\phi>1$) and varied the inlet temperatures to evaluate the influence on stability and emissions. A by-pass air was also used for dilution on post combustion zone. With this experiment they found that increasing inlet temperature improves the combustion efficiency but also increases NO_x emissions. These emissions decrease with the increase of equivalence ratio, except when using the by-pass air. The use of post combustion air gives higher values of NO_x due to its interaction with the hot unburned ammonia present in the post combustion zone, supported by numerical data. These results support the capability of this

blend to be used in gas turbines, however with low efficiencies which may need new injection techniques to reduce NO_x/unburned NH_3 in flue gases.

Following the same work line as Valera Medina and his co-workers, a group from Japan performed a series of experiments with swirl combustion to operate with ammonia.

In 2017, Hayakawa et al. [25] still using premixed ammonia/air flames, at atmospheric pressure, conducted tests to assess the effects of burner geometry and swirl number on flame stability. They used 2 liner geometries to confine the flame, cylindrical and squared, 2 liner lengths, 2 swirl numbers and varied the inlet velocity. It was possible to stabilize the flame for various equivalence ratios and inlet velocities and their findings led them to conclude that swirl number and liner geometry have influence on blow off limits, however, the liner length doesn't affect these limits. They also did some measurements of NO, NH_3 and H_2 emissions where they observed that NO concentration decreased for rich conditions, but NH_3 and H_2 concentrations started to increase to unacceptable values. Meanwhile they found that for a slightly rich equivalence ratio, ϕ=1.05, ammonia and NO concentrations are similar.

In sequence and having in mind the conclusion from Valera Medina [22] that fully premixed reactants injection probably is not the best option and considering the promising results from [20], the Japanese group came with something new. Kurata et al. [26] claimed to be the first time that NH_3-air combustion power generation has been successfully achieved. For this experiment they used a 50 kW micro gas turbine system applying combustion techniques such as 2 stage diffusion-flame type combustor, heat-regenerative cycle, swirl flow mixing and selective catalytic reduction (SCR) for NO_x reduction. They examined the operation range, combustion and thermal efficiencies, exhaust gas analysis and NO conversion. The results gave, without any additives or pre-cracked H_2, a maximum electric power of 44.44 kW (Figure 1.7 (a)) with combustion efficiency from 89% to 96% for NH_3-air combustion. They found out that NO_x and unburnt NH_3 emission are strongly dependent on combustion inlet temperature (CIT) (Figure 1.7 (b)) and observed the presence of both in the exhaust gases which led them to conclude that there are a NH_3 rich region, which releases NH_3, and a NH_3 lean region, which produces NO, in the primary combustion zone. Afterwards in the secondary zone, they expected that the unburnt NH_3 reduces the produced NO through the selective non catalytic reduction (SNCR) because the temperature in this region is within the range for that mechanism to occur (850-1150 ºC). They also performed tests with NH_3-CH_4 mixtures and noticed that the increase of NH_3 in the fuel ratio increases the NO emission until a NH_3 fuel ratio around 0.65 and after that, an increase of NH_3 decreases NO emissions due to reduction by residual NH_3 (Figure 1.7 (c)). For both blends the efficiency increases with power increase and with CIT increase, showing the importance of regenerative cycles in gas-turbine power generation.

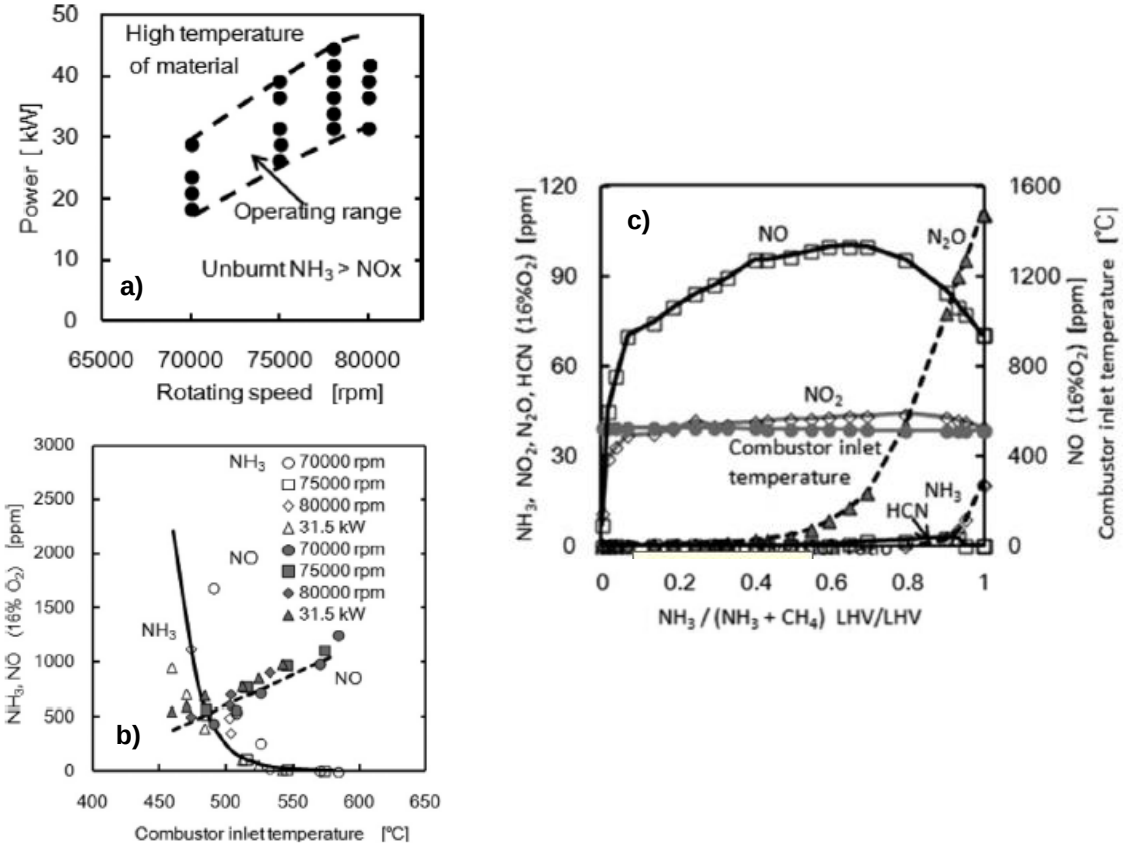

Figure 1.7 – (a) operation range for NH_3/air combustion, (b) variation of NO_x and NH_3 emissions with CIT before SCR, (c) species concentrations for varied NH_3 fuel ratio in NH_3/CH_4/air combustion. Adapted from [26].

Later, complementing the previous work [26], Okafor et al. [27] used the same combustor to perform their combustion tests. They investigated the effects of fuel injection angle, combustion inlet temperature (CIT), equivalence ratio and ambient pressure on flame stabilization and emission for non-premixed combustion. This work helped them to find that combustion efficiency can be improved using swirl and inclined fuel-injection, instead of traditional vertical injection, due to the better mixing of reactants and bigger fluid residence time in the combustor resulting from these techniques, giving also lower emissions. The use of 3D simulations helped them to conclude that an equivalence ratio control, which may control O/H radical profiles, is critical to the control of fuel NO_x emissions. The increase of ambient pressure promotes a decrease in O/H radicals concentration, therefore a decrease in NO_x emissions, indicating that ambient pressure is also an important factor for low NO_x emissions. With the use of a two-stage combustor in their work, they found that slightly rich equivalence ratio (1.1) in the primary zone resulted in the lowest NO_x emissions. The experiments showed that for lean combustion in primary zone, NO_x emissions are high due high NO production in this zone and for rich combustion, ϕ>1.1, NO production in the primary zone is very low, however significant amounts of unburned NH_3 and H_2 are transported and burned in the secondary zone leading to high NO production there. In this study it was recorded 42 ppm V NO_x emission with 99.5% of combustion efficiency at CIT of 298 K for 31.44 KW of fuel input power.

Alongside their own experiments, both Valera Medina group and the Japanese group did some research work and published papers with an overview of the ammonia combustion experiments and technologies already explored before them.

In 2018, Kobayashi et al [2] did a good work on explaining and resuming the most important features when dealing with ammonia combustion. After a brief introduction talking about the need for new "carbon free" fuels, his paperwork appoints the reasons why ammonia should be considered as a fuel and explicit their current situation on NH_3 research in Japan, where the need of new power sources for electricity production with low GHG emission are extremely needed since the accident at Fukushima nuclear power plant in 2011. Afterwards, their work resumes and quotes numerous works about fundamentals of ammonia combustion, more specifically NH_3/air premixed flames characteristics, comparisons with CH_4/air flames and flame enhancement, by H_2 addition, fossil fuel addition, oxygen enrichment flames, etc. They also reviewed many different chemical kinetics mechanisms used for prediction and validation of ammonia oxidation and NO_x formation. In the end, an analysis of the experimental work was done by the authors based on the work done by them towards a development of low-NO_x NH_3 fuelled gas turbine [27] at the research national institute of advanced industrial science and technology, concluding that the combustion research community should continue to develop the NH_3 combustion systems.

In the same time, Valera Medina et al. [3] did an extensive review of the works using ammonia. After giving some insights of ammonia usage and its challenges, the authors resumed the experiments, technologies and conclusions came from many different work groups throughout the past years on ammonia for power generation. These works cover ammonia usage in power cycles, fuel cells, gas turbines, combustion engines, etc. This work has a chapter where the authors mentioned various works done on ammonia combustion fundamentals and flame characteristics with also references to the chemical kinetics models developed for the study of ammonia combustion. With this review the authors demonstrate the wide possibilities of using ammonia for power generation, giving more strength to the idea of ammonia as an actual alternative clean fuel.

In 2020, Abdulrahman A. Khateeb et al. [28] showed his results of his work on ammonia-methane-air flames burning in a laboratory swirl combustor. The authors evaluated the stability limits of these flames, doing first an assessment of the limits of methane-air flames using the same burner for further comparison. The main difference between these two types of flames is that both the maximum and minimum equivalence ratios for a chosen condition increase with the increase of ammonia in the fuel mixture widening the stable region. However, while for methane-air flames the maximum equivalence ratio is controlled by flashback phenomena, for ammonia-methane-air flames the maximum values are controlled by flashback until a certain ammonia fraction ($\sim x_{NH_3} = 0.5$) and occurring rich blowout for further increase, resulting in a larger stable region for $x_{NH_3} > 0.5$ (Figure 1.8). The author also measured exhaust NO, observing that NO emission decreased with the increase of NH3 addition for a fixed equivalence ratio. He also noticed that low NO concentration only could be reached for slightly rich ammonia-methane-air mixtures. It´s worth noting that in this study the author could stabilize pure

ammonia-air flames for equivalence ratios between 0.79 and 1.24 which is a good perspective towards pure ammonia burner technologies.

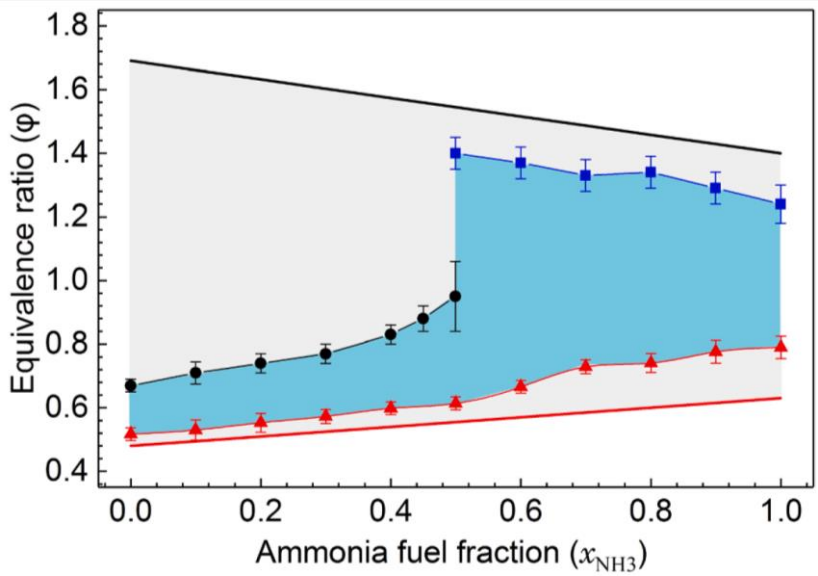

Figure 1.8 - Stability limits of ammonia-methane-air swirl flames as a function of the ammonia fuel fraction. The blue area shows the flame stability range bounded by lean blowout (red triangles), flashback (black circles), or rich blowout (blue squares). Adapted from [28].

Recently in IST, C. Filipe Ramos et al. [29] did previous experiments on ammonia combustion to evaluate the gaseous pollutant emissions. For their experiments it was used a premixed laminar flat flame burner at a fixed thermal input of 300W fuelled with CH_4/NH_3 mixtures. Both equivalence ratio and NH_3 molar fraction in the mixture were varied to investigate their influence on emissions. In general, the authors found high quantities of NO_x for all tested conditions and noticed that NO_x emissions decreased as the equivalence ratio is reduced towards fuel-lean conditions. CO and NH_3 emissions were found quite low for all conditions, indicating good fuel conversion. They also performed temperature measurements along the burner axis and beside the expected temperature decrease along the axial distance, they observed that the temperature profiles increased with the increase of NH_3 amount present in the fuel mixture. Additionally, the authors made some comparisons of the experimental results obtained with some kinetic simulations using different chemical kinetic mechanisms, which showed fair agreement between them.

1.3. Objectives

It is in this context, and having in mind the difficulties of ammonia combustion, that a new burner was designed and manufactured with the purpose of burning ammonia for our laboratory. This burner was designed to combine combustion stabilization techniques such as recirculation created by a bluff-body and swirl flow of the combustion air in a non-premixed combustion approach.

The following work is focused on this new burner, trying to characterize it and investigate its possible operational conditions. Give the flammability limits for different conditions and try to see how they vary with the thermal input and fuel composition.

Later temperature and species measurements are intended to be done not only for the exit of the combustor but also for a wide range of points inside the combustor, giving some in-flame data. The measurements should also cover different equivalence ratios and fuel compositions to see their influence both in temperature and emissions

With these experiments and measurements, it will be possible to conclude about the feasibility of the burner developed and its success on burning mixtures with high content of ammonia with higher thermal inputs than the ones used before in our laboratory [29].

These extensive measurements aimed to supply data for comparison and improvement of the numerical models that try to simulate the ammonia combusting, complementing the literature on that subject.

2 Theoretical Background

2.1. Chemistry

To try to understand some phenomena behind ammonia (NH_3) combustion, it is necessary to know some basic chemistry of burning it. Basically, as any other combustion processes, NH_3 needs an oxidizer, normally oxygen (O_2). To accomplish that it is more common to use air as the oxidizer, which also contains nitrogen (N_2) in a proportion of 1:3.76 in terms of molecules of O_2 to N_2. The reaction of burning ammonia can be represented as [6]:

$$4\,NH_3 + 3\,(O_2 + 3.76\,N_2) \rightarrow 6\,H_2O + 15.28\,N_2 \quad (1)$$

The equilibrium reaction stated in Equation (1 shows the ideal reaction of burning ammonia, which gives only H_2O and N_2 as products. This would be perfect since there is no CO_2 production, because of the carbon free nature of NH_3, and both combustion products are not harmful for the environment. However other reaction could be happening [6]:

$$4\,NH_3 + 5\,(O_2 + 3.76\,N_2) \rightarrow 4NO + 6\,H_2O + 18.8\,N_2 \quad (2)$$

It is from this reaction (2) that can be explained the existence of nitric oxide (NO) in products of NH_3 combustion. Moreover, the amount of NO present in exhaust gases from ammonia combustion does not come only from the reaction in (2, it could come also from the oxidation of the N_2 present in the air, due to the high temperatures in the flames by the so-called “Zel’dovich mechanism” [30]:

$$N_2 + O_2 \rightarrow 2NO \quad (3)$$

Despite that, NH_3 still is the main source of NO in ammonia combustion, which is called fuel-NO_x. Once NO is formed, it could lead to the formation of nitric dioxide (NO_2) and together they formed the main NO_x, which is the designation used for the nitric oxides produced during combustion. The formation of NO_2 can be represented [30]:

$$2NO + O_2 \rightarrow 2NO_2 \quad (4)$$

When the fuel is a mixture of NH_3 and H_2, the reaction could be represented by the following equation:

$$x\,NH3 + (1-x)H2 + (0.25x + 0.5)(O2 + 3.76\,N2) \rightarrow (0.5x + 1)\,H2O + (1.44x + 1.88)\,N2\ ; \quad (5)$$

where x represent the mole fraction of NH_3 in the fuel and it influences the resultant combustion products.

Concerning the NO_x, they are the main pollutants resulting from NH_3-H_2 mixture combustion, however, there are some techniques developed through the years to reduce the NO_x emissions, namely selective catalytic reduction (SCR) and selective non-catalytic reduction (SNCR).

The latest consists in the introduction of ammonia (or urea), in the post combustion zone, after NO formation, to react and convert it in water vapour and nitrogen. There are many reactions involved, but the overall reaction could be expressed as [30,31]:

$$4NO + 4NH_3 + O_2 \rightarrow 4N_2 + 6H_2O\,; \quad (6)$$

in case of using ammonia, or

$$H_2NCONH_2 + 2NO + \frac{1}{2}O2 \rightarrow 2N_2 + CO_2 + 2\,H_2O\,; \quad (7)$$

in case of using urea.

As it can be seen in Equation (7 the use of urea to reduce NO_x emissions will produce CO_2 emission, which is not desirable since it jeopardizes the potential of ammonia as carbon free fuel.

Regarding the SCR mechanisms, the effect is similar to SNCR, however it uses a catalyst in the post combustion zone. Despite some secondary reactions , depending on the catalyst or method used, the overall reaction is the same as in (6, when using ammonia, however the temperatures needed for the reaction to happen are much lower than in the SNCR case [30,31].

2.2. Stabilization techniques

Some stabilizations techniques were used in this work, as suggesting in the title. Regarding the use of bluff-body, the stabilization is obtained by the existence of a strong recirculation zone, where in theory contains burned products at approximately uniform temperature. There are some theories about the recirculation zone, being the one assuming that this zone behaves as a perfectly stirred reactor (PSR) the most adequate for this work. In this theory, a great amount of energy release is required when the unburned gases interact with the hot gases for the first time in the recirculation zone.

Figure 2.1 represents a schematic of the mechanism behind the creation of the recirculation with a bluff-body with the assumptions made.

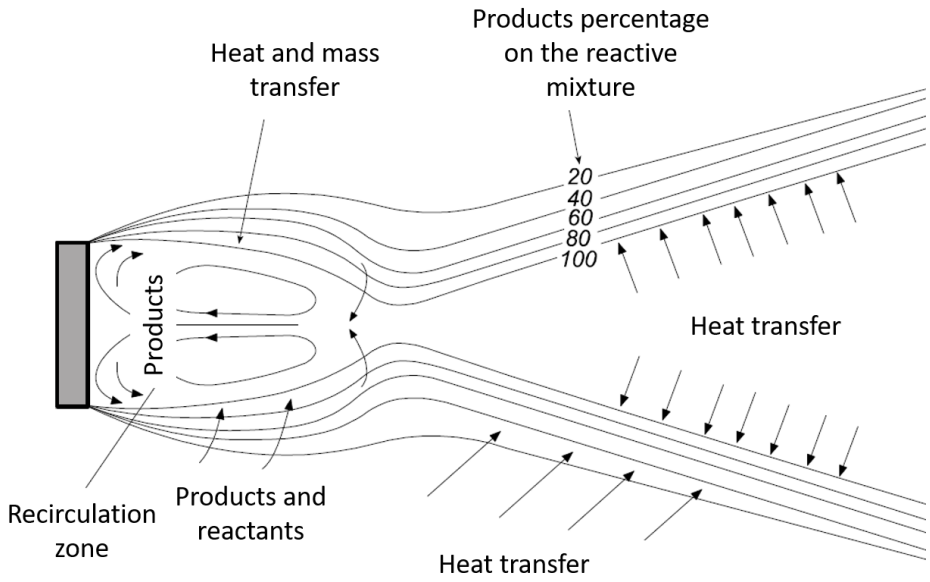

Figure 2.1 - Scheme of the recirculation zone created by a bluff body. Adapted from [32].

It was also applied swirl for flame stabilization. The mechanism behind is creating, near to the combustor axis, a zone of low velocity which may lead to the creation of the recirculation zone. The swirl could be achieved by using fixed blades, with a certain degree of inclination, mounted at the injection point, or it could be achieved by the injection of one of the reactants (usually air) normally or at a certain angle relatively to the combustor axis.

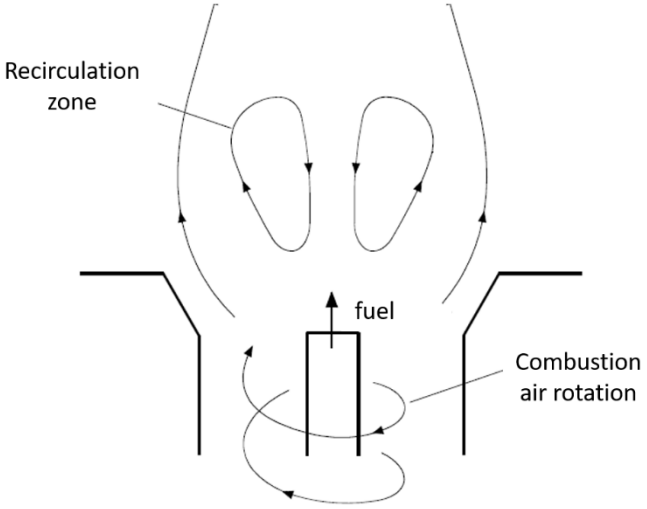

Figure 2.2 - Recirculation zone created by the rotation of the air combustion (swirl). Adapted from [32].

Additionally, for the non-premixed flames, swirl does not only promote the mixture of products and reactants but also improves the mixing of the fuel and the oxidizer. Also, controlling the swirl, it could be possible to control the flame length. The increase of the swirl, as already mentioned, will improve the reactants mixing, reducing the flame length.

3 Materials and methods

3.1. Experimental setup

3.1.1. Burner

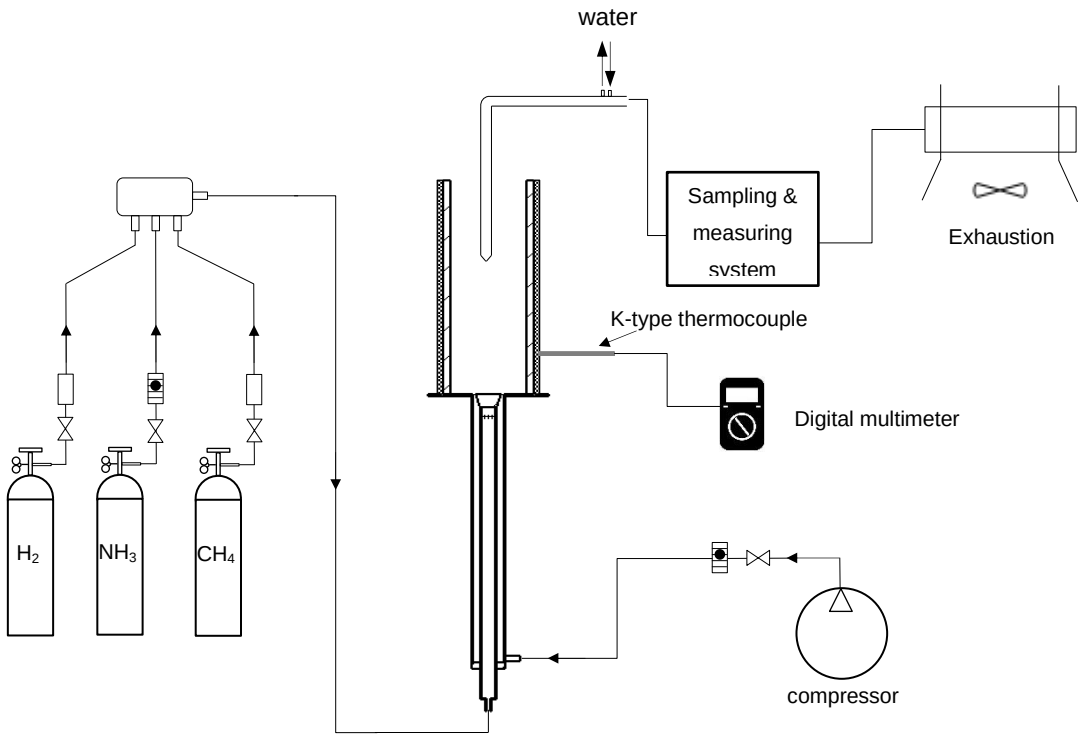

Figure 3.1 - Schematic of the burner setup.

Figure 3.1 shows the schematic layout of the experimental setup used in this work. Distinct parts can be easily identified, like the fuel supply, the burner itself and the sampling and measuring system.

Compressed bottles were used for fuel supplying, one for NH_3 and another for H_2. As for the CH_4 supply, it comes from the common supply line in the laboratory and it is represented in the scheme as a bottle for simplification. At the exit of the compressed bottles there is a pressure regulator to control and set the desired pressure. The NH_3 flow rate is controlled by fluctuating rotameter (ABB, model 10A6131C) while the H_2 and CH_4 flow rates are controlled by digital flow meters (Aalborg, model GFM 17 and OMEGA, model FMA-A2317 respectively). After the fuels pass through the flow meters, they are conducted through Teflon tubes into the burner, being mixed before injection.

Additionally, air is supplied from the compressor, also passing through a pressure regulator and the flow rate is set using a fluctuating rotameter (Fischer & Porter, model 10A1197).

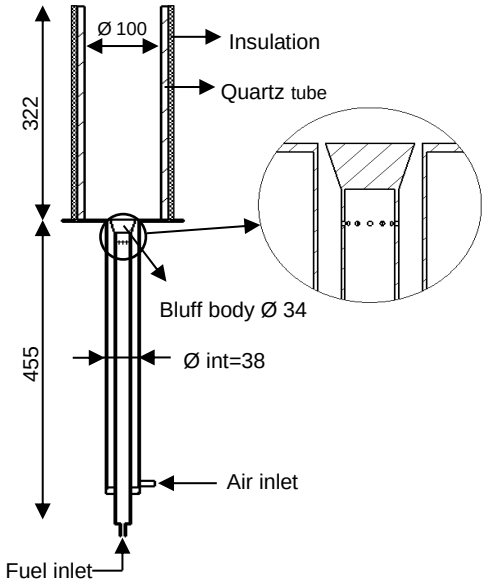

Figure 3.2 - Detailed scheme of the burner. All values are in mm.

The burner is represented with more detail in Figure 3.2. It consists of two co-axial tubes for fuel and air injection, a bluff body at the exit to achieve recirculation and a quartz tube to confine the flame.

As it can be seen in Figure 3.2, the air is injected in the tangential direction to create a swirl circulation. For that the air is injected in the outer tube, with internal diameter of 38 mm, through two smaller tubes with internal diameter of 6 mm. In its turn, the fuel mixture (NH_3 and H_2) runs through the inner tube, with outer diameter of 22 mm and 2 mm of thickness, being injected radially, through 12 holes with 2 mm of diameter, into the air flow around 13.5 mm below the bluff body.

The bluff body used in this work has a height of 20 mm, a base diameter of 22 mm and a top diameter of 34 mm. As mentioned before, the bluff body is placed after de fuel and air injection and it is meant to be an obstacle to their flow with the intention of creating some recirculation improving the air and fuel mixture.

At the level of the end of the bluff body, a quartz tube is placed with 100 mm of internal diameter, 322 mm of height and 10 mm of thickness. This tube purpose is to provide a confinement to the flame and is insulated with a 20 mm ceramic wool to reduce heat losses.

Concerning the sampling and measuring systems, they will be discussed in the next sections, however, as it can be seen in Figure 3.1, a species probe is placed inside or at the exit of the quartz tube, to aspirate samples from the exhaust gas to be used in the measurements. All the exhaust gases that are not sampled, are extracted from the exhaustion that is placed over the burner setup. Also, instead of a species probe, it could be placed a thermocouple, according to the measurements being done.

3.1.2. Measuring equipment

3.1.2.1. Sampling and measuring system

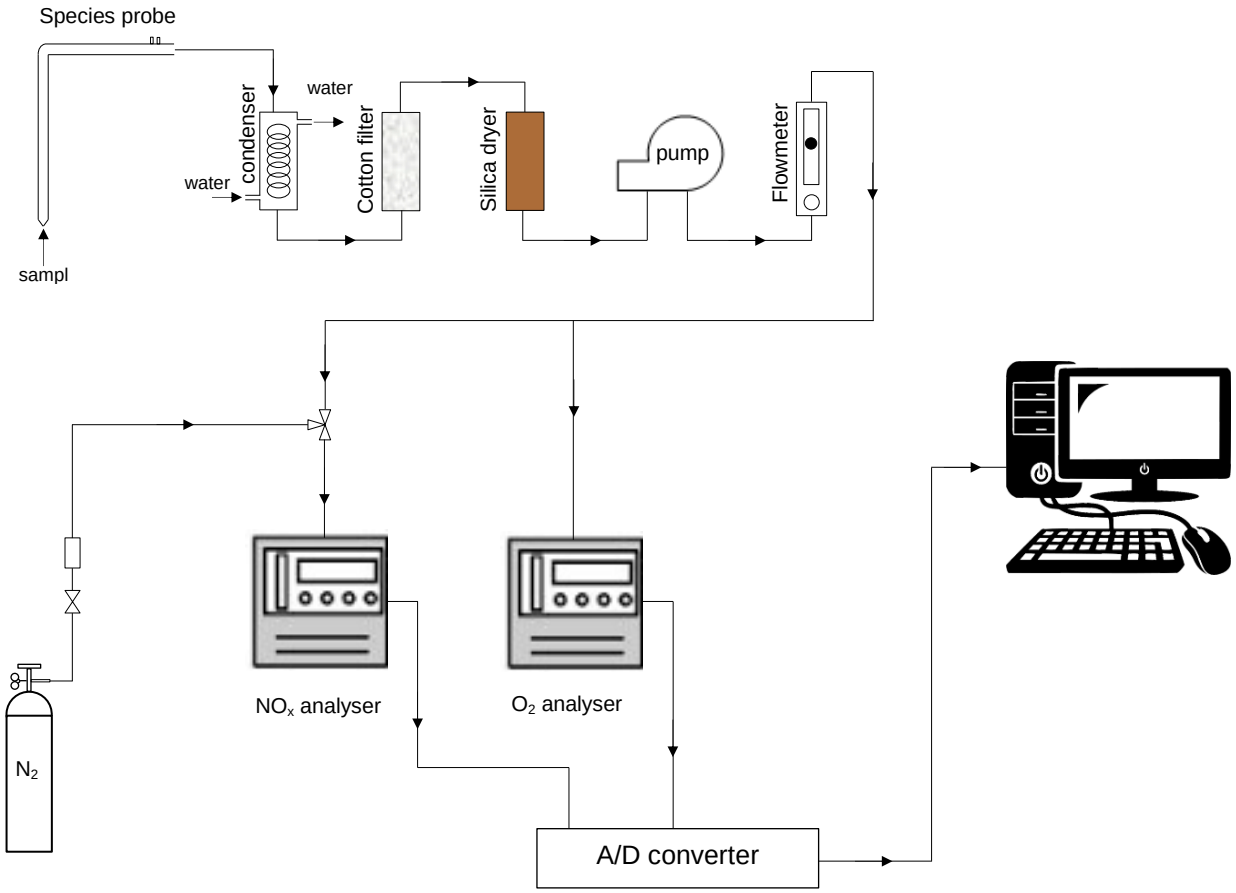

Figure 3.3 - Schematic of sampling and gas analysers system.

Figure 3.3 represents a schematic of the circuit and equipment used for measuring gas species, specifically NO_x and O_2. The sample is first collected in the species probe placed in the measuring position. To do that, the probe is fixed in a metallic structure which allows it to move in the vertical direction and in the radial direction inside the quartz tube. The species probe, Figure 3.4, is made of stainless steel with an inner channel where the gas sample runs through and another channel where water circulates to continuously cool the probe avoiding it to melt when experiencing high temperatures. Also, the gas sample is cooled while passing through the probe. Figure 3.4 represents the probe layout and its dimensions.

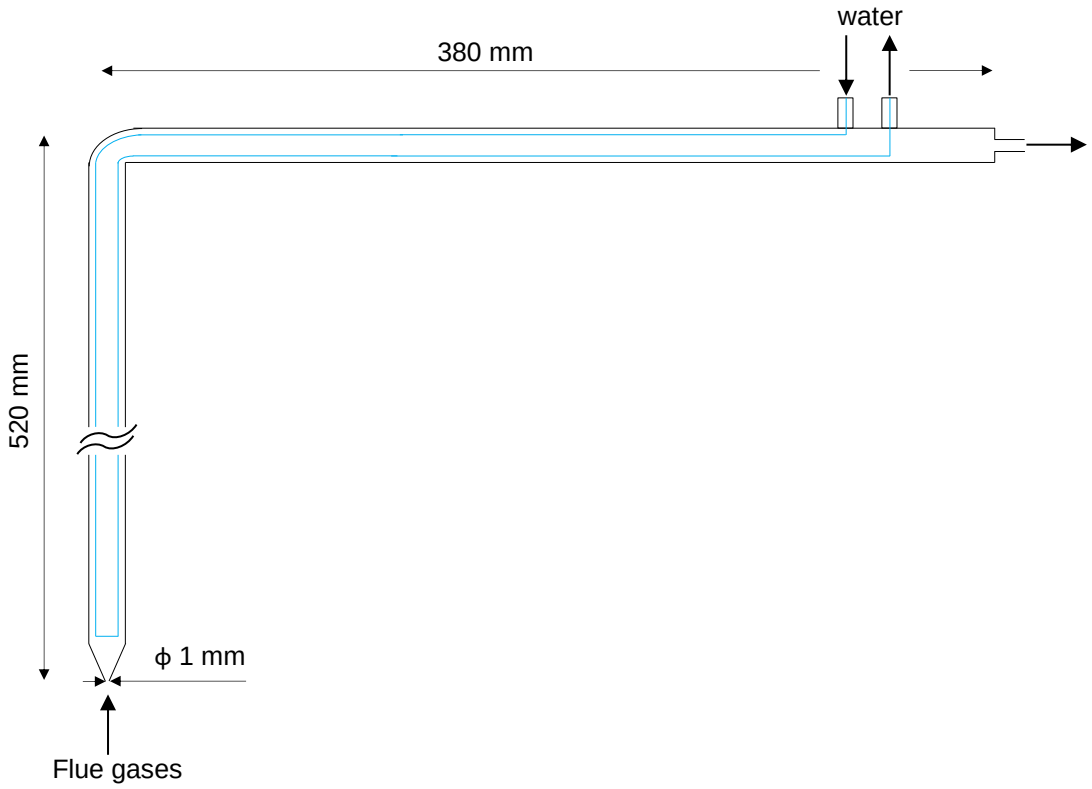

Figure 3.4 - Schematic of gas species probe. Blue lines represent the circuit done by the cooling water within the probe.

After exiting the species probe, the gas sample runs through a condenser, a cotton filter and a silica dryer to remove all the humidity and other impurities, ensuring that the sample is dry and clean when arriving at the gas analysers, giving the measurement values on a dry basis. In sequence, there is a pump and a flowmeter to ensure that the sample volume flow is kept constant during the measurements. Between all the components, from the exit of the probe to the exit of the flowmeter, the sample runs through Teflon tubes which don't react with the sample species and do not contaminate the sample.

Leaving the flowmeter, the gas sample is directed into the gas analysers. Two different analysers were used, one for measuring NO_x and another to measure O_2. The one used for NO_x is a chemiluminescence type Horiba CLA-510SS model with a value range of 0-2000 ppm vol. while the analyser used for O_2 is a paramagnetic type Horiba CMA-331A model with a value range of 0-25 % vol. The analysers create an electric analogue signal that is sent to an acquisition board (Data Translation DT9802) converting it to digital at a frequency of 100 Hz. The board is connected to the computer to register the sent data and a dedicated program is ran at a sampling period of 30s for each measurement, giving an average of 3000 instantaneous measurements each value recorded.

In some conditions the quantity of NOx present in the sample overcomes the maximum value detectable by the analyser. As shown in Figure 3.3, N_2 is introduced and mixed with the gas sample only before entering the NOx analyser to dilute it and bring the values of NO_x to within the scale.

3.1.2.2. NH_3 exhaust measurement system

When NH_3 exhaust emissions were measured, the use of analysers were not possible, because there was none that measures NH_3 in the laboratory and the system represented in Figure 3.5 was used.

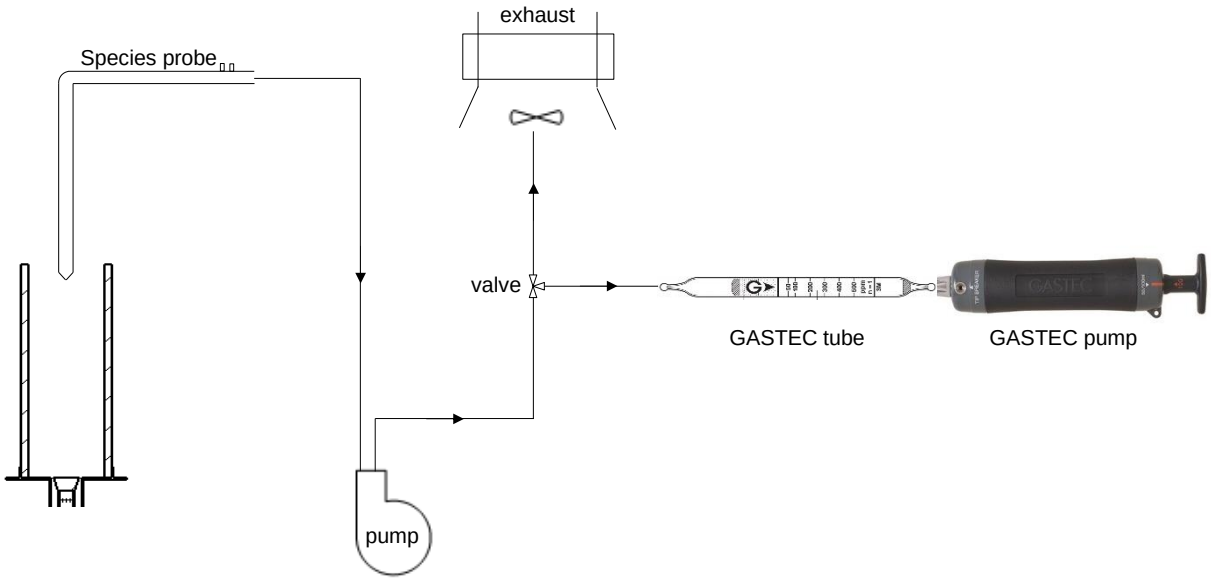

Figure 3.5 - Schematic of ammonia measuring system.

This was a more rudimentary way to measure gas species therefore with more uncertainty when compared with gas analysers. To perform these measurements, the species probe was placed at the exit of the tube quartz (h=300mm) and the pump is keeping the sampling flow constant. The sample runs through Teflon tubes between equipment until the exhaust. There is a bifurcation valve between the pump and the exhaust to allow the sample to shift his direction to a specific tube where the NH_3 measurement equipment is placed when the measurements are taking place. The measurement equipment is composed by a GASTEC detector tube and a GASTEC manual pump.

The manual pump is a Gastec GV-100S model which has two possible pump configurations, one pump stroke which samples 100 mL of gas and half-stroke sampling 50 mL. The detector tubes are attached to the pump for taking the measurements and the lever of the pump is pulled to make the sample pass through the tube into the pump.

There are different types of detector tubes, accordingly the scale needed, being Gastec 3M the one used. The detector tubes are thin glass tubes with a particulate matrix inside with a reagent (H_3PO_4) which is sensitive to the presence of NH_3 reacting with it shifting the colour of the matrix (Figure 3.6). The value of NH_3 present on the sample corresponds to the amount of colour shifting on the matrix that can be translated through the scale printed on the glass tube. The scale printed on the tube varies from 50-500 ppm for 1 stroke. However, according to the specifications of the tube, more strokes can be done to measure values lower than 50 ppm. In the same trend the maximum value measured could be increased to 1000 ppm if it is used 1 half-stroke.

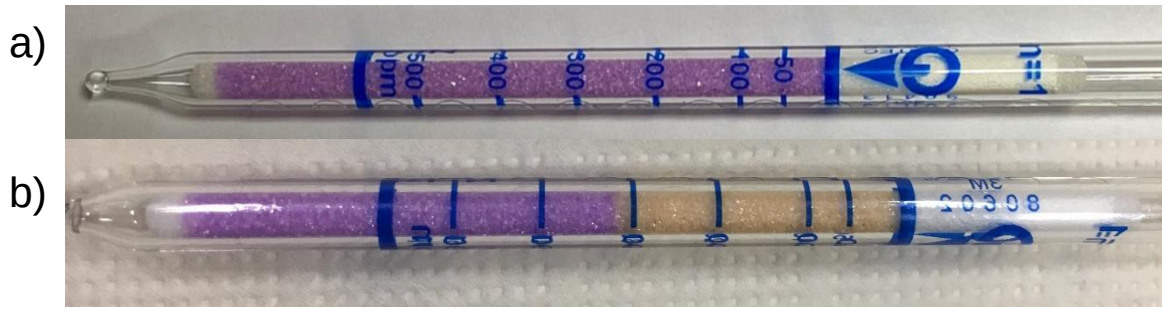

Figure 3.6 – Gastec tubes 3M. a) unused tube. b) used tube where it can be seen the colour shifting, measuring slightly more than 300 ppm.

3.1.2.3. Thermocouple

To take temperature measurements it was used a different system, represented in Figure 3.7, using a thermocouple, an amplifier and an A/D converter to read the values.

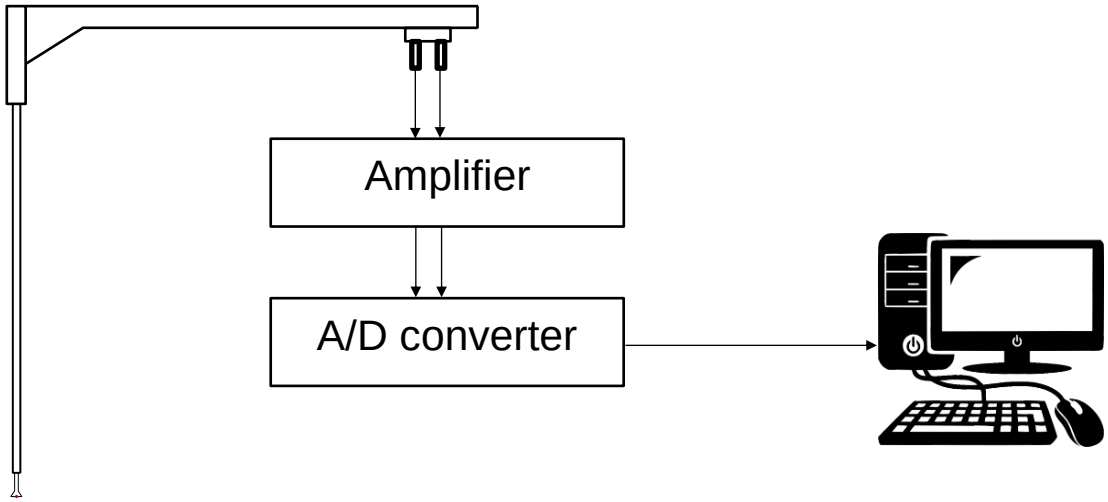

Figure 3.7 - Schematic of the temperature measuring system.

The thermocouple is composed by two wires of different metal alloys welded together at one specific point, called “hot joint”. When the joint is in contact with temperature variations it will produce an electrical potential difference depending on the temperature. The thermocouple used is composed with a platinum anode and a cathode made from an alloy of platinum with 13% of rhodium, which is commonly referred to as a Pt/Pt-13%Rh type R thermocouple. The range of values measured with this type of thermocouple goes from -50 to 1760 ºC which corresponds to potentials going from -0.226mV to 21.003mV according to International Thermocouple Reference Tables [33].

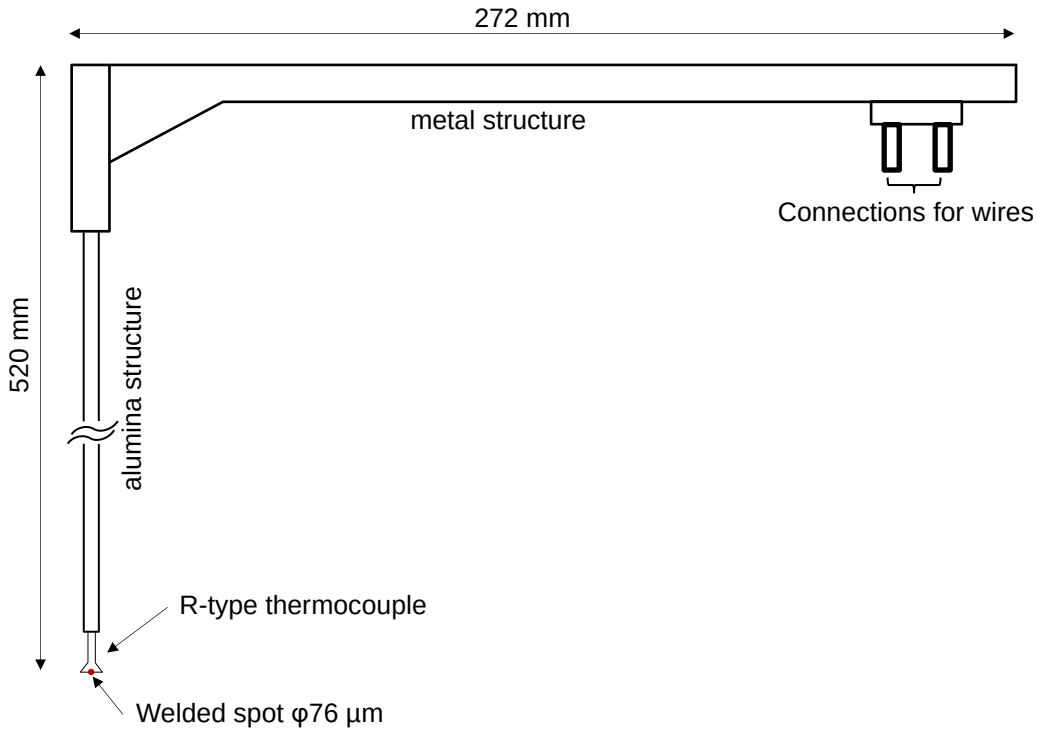

Figure 3.8 - Schematic of the thermocouple used in the temperature measuring system.

Figure 3.8 represents the configuration and dimensions of the thermocouple probe used in this work. This probe is attached to the same metallic structure as the species probe to allow the movement along the axis. The thermocouple is connected to two parallel wires made of the same materials of the thermocouple, which mean one of platinum and the other of platinum with 13% of rhodium, with larger diameter. These wires run through an alumina tube without any contact along it carrying the signal produced in the “hot joint”. In the end of the metal structure of the thermocouple the wires are connected to compensated wires which are connected to the amplifier, carrying the signal from the thermocouple to the amplifier (Data Translation 5B37-R-05), where it is filtered and amplified before being sent to the A/D converter (Data Translation DT9802). Then the signal is converted from analogue to digital and sent to the computer which uses a dedicated program to read the values. The sample acquisition is made at 100 Hz for 30 seconds.

3.2. Experimental procedure

3.2.1. Flame initiation

The first step before all types of experiences is the starting and stabilization of the flame. For that the compressor, the room ventilation, the exhaust gas extraction and the CH_4 and H_2 digital flow meters are turned on. Then, after checking if all valves and flow meters are closed, the CH_4 valve is open as well as the air valve, which is set with ~1 bar as pressure exit. The ignition is made with a CH_4/air flame, opening first the air flow meter supplying around 20 L/min, then the CH_4 flow meter supplying around 2 L/min and finally using a lighter to ignite the flame.

After all this, to warm up the quartz tube confinement, the CH_4/air flame is left burning until the exterior wall of the tube reaches a temperature around 420 ºC, which was found by experience to be a reasonable value from which temperature variations are relatively small, reducing the effect of temperature gradient on flame stabilization. Approximately one hour later, which is the time to reach the desired temperature, the NH_3 and H_2 gas bottles are opened, and their pressure regulators are also set with ~1bar exit pressure. The NH_3 and H_2 valves are then opened, increasing first the supply of NH_3 to around 1.6 L/min, also increasing the air supply to 25 L/min. After that, the procedure is basically increasing gradually the H_2, NH_3 and air supply, always looking at the flame to see if it remains stable, decreasing at the same time the CH_4 supply until there is no need of it for the flame to be stable. From experience with about 4.5 L/min of NH_3, 0.75 L/min of H_2 and 32 L/min of air, the supply of CH_4 to the flame is no longer required.

At this point the NH_3/H_2/air flame is ready to be set at any desired test condition to perform all the tests contemplated in this work.

3.2.2. Stability tests

Once the NH_3/H_2/air flame is obtained and stabilized, as described in section 3.2.1, it is possible to start the stability tests. 3 different thermal inputs were used, 0.7, 1.3 and 1.9 kW, and the molar fraction of NH_3 in the fuel (x_{NH_3}), defined as $x_{NH_3} = V_{NH_3}/(V_{NH_3} + V_{H_2})$, was varied from 0.5 to 1. After choosing one of the conditions, i.e. defining the thermal power and the value of x_{NH_3}, the flows of NH_3 and H_2 are set to the calculated value for this condition and keeping these values constant, the air flow was decreased or increased until extinction or unstable regime was observed, giving the maximum (rich limit) and the minimum (lean limit) equivalence ratio (ϕ) for each condition , respectively. The tests for each condition were repeated, at least, 3 times to verify the repeatability of the results.

3.2.3. Temperature measurements

The measurements were taken only for selected conditions, present in Table 4.1, and its goal is to assess the temperature within the quartz cylinder both in axial (z) and radial (r) direction (Figure 3.9).

To perform this kind of test, the thermocouple described in section 3.1.2.3 was used, which is secure in a metallic structure that has two endless threads to enable the motion of the thermocouple in the 2 desired directions. As stability tests, the temperature measurements can be started after the procedure described in section 3.2.1, but before that, the thermocouple is centred. After the NH_3/H_2/air flame is established in the chosen condition, the thermocouple is then driven throughout the inside of the cylinder and the temperature is recorded for all predetermined points, i.e. all r and z couples. The magnitude of motion in both directions is measured by rulers attached in the metallic structure. The temperature in each point was recorded, at least, 3 times for all conditions.

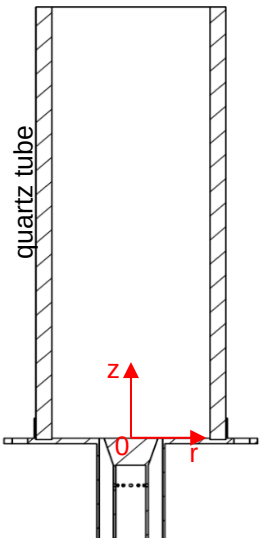

Figure 3.9 – Referential used for the measurement points. z is the axial axis and r the radial axis.

3.2.4. Species measurements

3.2.4.1. NO_x and O_2 measurements

For these measurements the same conditions as in the temperature measurements were used, Table 4.1. The probe, analysers and sampling system as described in section 3.1.2.1. were also used. The probe is secured in the same metallic structure as the thermocouple, allowing it to move in the same directions and therefore the probe can be put in the same points as the thermocouple.

The probe is centered before flame initiation, section 3.2.1, then the condition to be measured is set up. After that, and before introducing the probe inside the quartz tube, the cooling water valve is opened. Then the probe is placed in the measuring points to recoil samples that are sent to the analysers and record their values of NO_x and O_2. After one-point measurement was finished, the probe was moved to

another point and it was needed about 5 minutes to allow the stabilization of the analyser readings and start taking the measurements of the new point.

If dilution is needed, i.e. when the value of NO_x exceeds the analyser scale, N_2 bottle is opened and the flow is gradually increased until the value is within the scale. Then all measurements were taken with constant N_2 flow and in the end, using a calibration bottle, the rate of dilution is determined. For each point of each condition it was taken, at least, 6 values of both species.

3.2.4.2. NH_3 measurements

As the previous, NH_3 measurements were taken for the same conditions, Table 4.1, but only for the exit of the cylinder. To perform these measurements, the equipment as described in section 3.1.2.2. was used.

Like previously, the probe is centered before flame initiation, section 3.2.1, then the flame is set in the desired condition and the cooling water valve is open. After that, the probe is put at a height h = 300 mm and the pump is turned on, starting to aspirate the flue gases. Then the Gastec tube glass tips are broken and it is attached in the manual pump, according to the instructions, the valve in the nylon tube bifurcation is opened, the Gastec tube is introduced in the nylon tube and the needed strokes for recording the measurement of NH_3 were done. Once the value is visible, the valve is closed, the tube is separated from the manual pump, a picture of the tube is taken, the probe is elevated, and the pump is turned off. Before doing another measurement for a different condition the nylon tube is cleaned with compressed air blasting jets on the inside, then it is mounted again, and the system is ready for another measurement.

3.2.5. Finishing and closing the systems

Like the first step, the last step of all types of experiences is the same. Once finished the measurement, the intrusive measurement equipment (species probe or thermocouple) are removed from the inside of the quartz tube and the NH_3/H_2/air flame is set with about 4.5 L/min of NH_3, 1 L/min of H_2 and 32 L/min of air. At this point the CH_4 flow meter is open supplying around 1.5 L/min. After that the pressurized bottles could be closed to purge the fuel supply line. The H_2 bottle is closed first and when the pressure regulator at the exit of the bottle shows no pressure and the H_2 flow meter shows no flow, it means that there is no hydrogen left and both can be closed. The same procedure is done to the NH_3 bottle, decreasing the air flow to 25 L/min. Then, the CH_4 supplying valve is closed, extinguishing the remaining CH_4/air flame, both air and CH_4 flow meters are closed and the air valve is closed. The cooling water, if it was used, is left running for a few minutes to cool the species probe. Finally, after checking if all bottles, valves and flow meters are closed, the water valve is closed and the compressor, the CH_4 and H_2 flow meters, the room ventilation and the exhaust gas extraction are turned off.

3.3. Experimental uncertainties

3.3.1. Relative to flow meters

The uncertainties related to the gas flow meters readings can be evaluated to be sure if the values set up experimentally are too different of the ones that could be the real ones. These uncertainties of the flow meters, in this case, will be relevant when setting the equivalence ratio and the quantity of NH_3, or H_2, in the fuel that is intended to work with.

For these cases, the combined standard uncertainty can be calculated by [34]:

$$u_c{}^2 = \sum_{i=1}^{N} \left(\frac{\partial p}{\partial x_i}\right)^2 u^2(x_i) \tag{8}$$

Where u_c is the combined uncertainty, x_i the variable being analysed, p the function of the variable being analysed and u the standard uncertainty associated with the equipment.

$$x_{NH_3} = \frac{V_{NH_3}}{V_{NH_3} + V_{H_2}} \tag{9}$$

Equation (9 is used to determine the quantity of NH_3 in the fuel mixture, where x_{NH_3} is the molar fraction of NH_3, V_{NH_3} is the Volumetric flow rate of NH_3 and V_{H_2} is the volumetric flow of H_2.

Having both Equation (8 and Equation (9 in mind and knowing that the NH_3 flow meter and H2 flow meter have a relative uncertainty, respectively, of 5% and 1.5% of the full scale, the maximum combined uncertainty when setting the fuel conditions (x_{NH_3}) is about 4.4 % between all the conditions used.

$$\varphi = \frac{(A/F)_{st}}{(A/F)_{used}} = \frac{(A/F)_{st}}{\frac{Air\ used}{Fuel\ used}} \tag{10}$$

Equation (10 is used to set the equivalence ratio used, where $(A/F)_{st}$ is the ratio between air and fuel used for stoichiometric combustion (ϕ=1).

Using again Equation (8 combined with Equation (10 and knowing that the average relative uncertainty of the air flow meter is about 2% of the measured value, the maximum uncertainty when setting the equivalence ratio to be used is still about 2%.

3.3.2. Temperatures

For the temperatures, the standard uncertainty for the R type thermocouples is ± 1.5 ºC or ± 0.25% of the measured value, whichever is greater. Since the uncertainty comes directly from the variable measurements the derivative term of Equation (8 is equal to 1. Therefore, the error can be calculated from the equation below.

$$u_c{}^2 = u^2 + u_s{}^2 \tag{11}$$

Equation (11 was used to give a combined uncertainty (u_c) between the instrument scale uncertainty (u) and the standard deviation (u_s) resulting from the different measurements taken for each value obtained. The standard deviation was calculated by:

$$u_s = \sqrt{\frac{\sum(x_j - \mu)^2}{N}} \tag{12}$$

Where x_j is the value measured in each j repetition, μ is the mean value of the repetitions, and N is the number of measurements taken. Using Equation (11 the maximum relative uncertainty for the temperatures was about 2%.

It is worth to mention that also the position of the probe used has also an error associated since it was used measuring tape to control it. Therefore, it can be assumed that the probe position has an uncertainty of ± 0.5 mm.

3.3.3. Gas species concentrations

Regarding the measurements of the species, more exactly NO_x and O_2, it is valid the same justification as for the temperatures and Equation (11 was used to find the uncertainties of these measurements.

For the case of NO_x measurements, the uncertainty relative to the analyser is ± 0.05% of the full scale, which gives an uncertainty of ± 10 ppm. Using Equation (11, the maximum combined relative uncertainty is 18%.

For O_2 measurements, the analyser uncertainty is also ± 0.05 % of the full scale, which gives ± 0.125% of uncertainty. Using Equation (11 the maximum relative uncertainty was 14%.

When measuring the NH_3, the uncertainty was estimated by the uncertainty relative to the equipment used, which is ± 5% of the measured values which can correspond to a maximum absolute deviation of ± 50 ppm.

All estimated uncertainties are summarized in Table 3.1.

Table 3.1 - Summary of the uncertainties estimated for the parameters evaluated in this work.

Parameter evaluated	Uncertainty
x_{NH_3}	4.4 %
ϕ	2%
temperature	2%
NO_x	18%
O_2	14%
NH_3	± 50 ppm

4 Results and discussion

4.1. Stability

Once the burner was developed for this work, tests to assess its stability limits were taken in the first place to give the operational range of work and help defining the conditions to be studied in the next experiments/measurements.

As states in 3.1.1 the bluff body used for the experiments has a top diameter of 34 mm, however, first attempts to use this new burner were made with a bluff body with top diameter of 30 mm. Doing some trials and based essentially on flame observation it was concluded that the stability was not as good as desired and then, the bluff body diameter was increased to increase the exit velocity of the partial pre-mixed fuel-air mixture and by its turn increase the stability of the flame. Later tests were made with bluff bodies larger than 34 mm and it was observed that the stability limits decreased, probably because of instabilities caused by the higher velocities and the small gap between the bluff body and the outer tube internal wall.

After selecting the bluff-body (34 mm), to perform the experiments, three different thermal inputs (0.7, 1.3, 1.9 kW) were selected and the quantity of NH_3 in the fuel mixture (by volume) was varied from 50% to 100% with 10% increments.

A sort of preliminary test was made to assess the effect of insulation of the quartz tube in the stability of the flame. First measures of the rich and lean stability limits were performed without any insulation being repeated after with insulation.

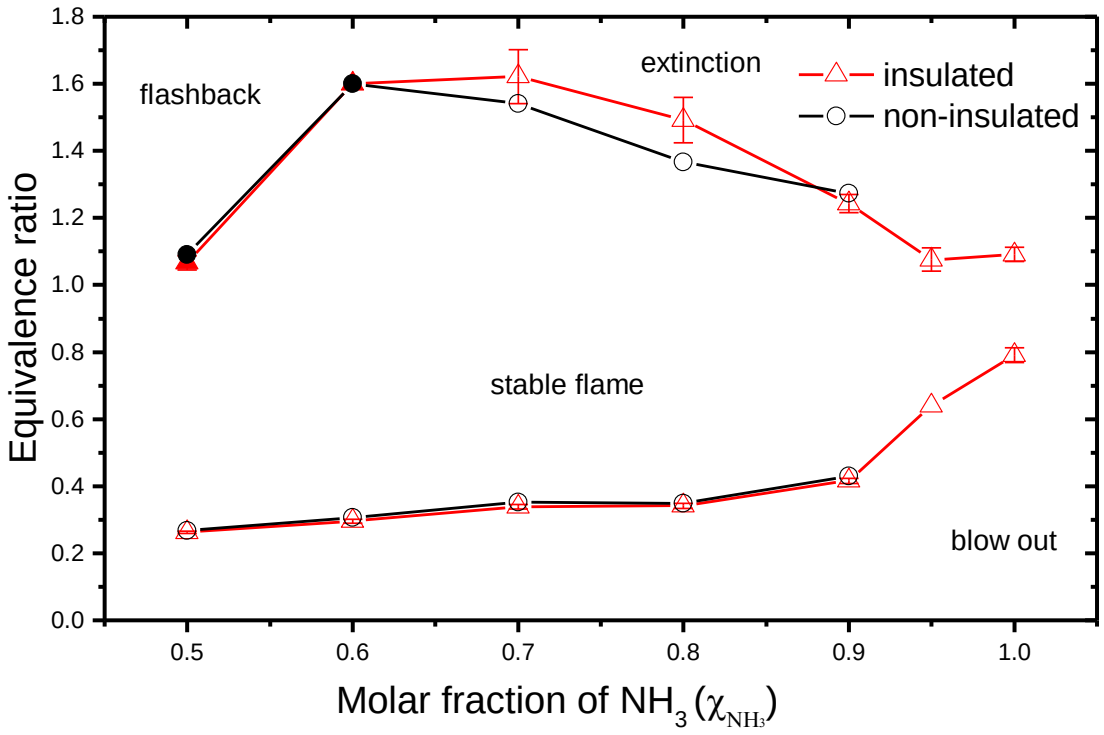

Figure 4.1- Comparison of the flame stability between insulated and non-insulated combustor for 1.9kW.

Looking to Figure 4.1 it can be seen that for the lean flammability limit the difference between insulated and non-insulated values is not significant. This could mean that the reason for flame extinction in this case is more dependent on burner geometry and the injection velocities than the heat losses. As it concerns to the rich flammability limit, for the points where flashback occurred, the limit values were similar, meaning again that here it is more dependent on the velocities and reactivity of the mixture. For ϕ = 0.7 and 0.8 is where it can be seen some significant differences. Here, in conditions with less reactivity, we can assume that the heat losses play a major role in the flame extinction, where the rich flammability limit can be improved by reducing the heat losses by means of insulation. Also, without insulation stabilizing flames with more than 90% of NH_3 was practically impossible, while with insulation it could be done but still with small range of operation.

After this, it was decided to use insulation for the experiments that followed. The stability tests were performed as described in 3.2.2 being the results shown in the following graph.

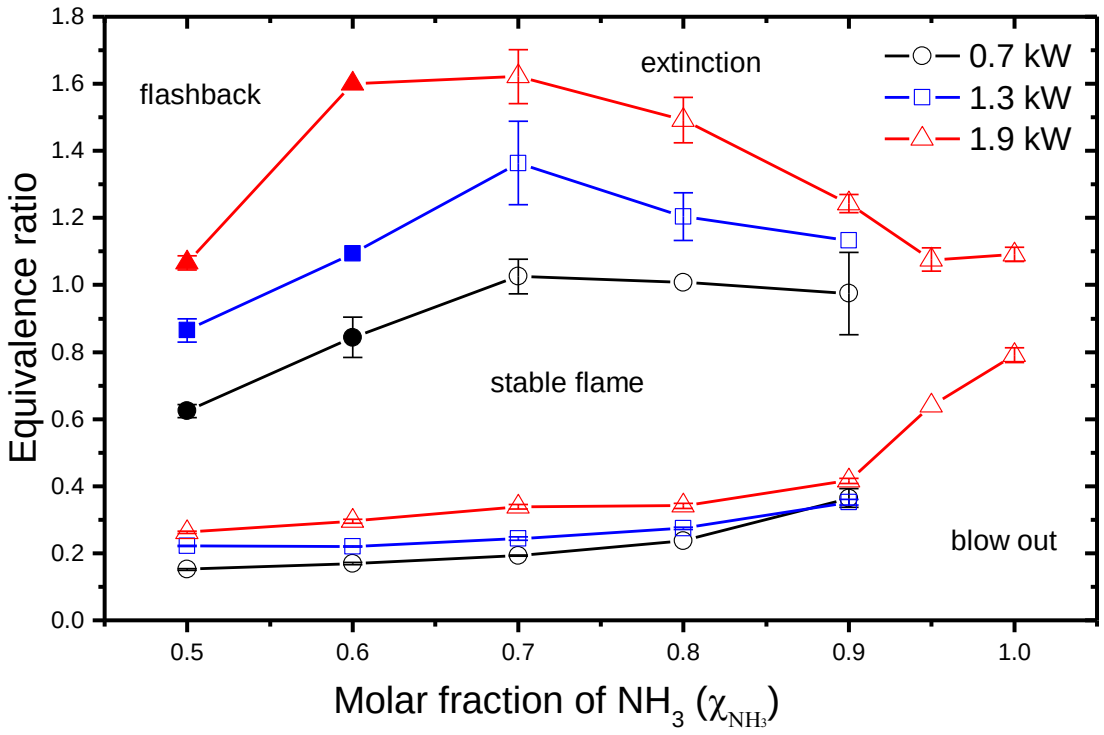

Figure 4.2 - Stability diagram for the thermal inputs studied. Filled symbols refer to the points where flashback occurred.

Figure 4.2 represents the graph resulting from the stability tests done. Some conclusions can be drawn from there, but it is worth noting first that the use of more than 90% of NH_3 was only achieved for the maximum thermal input, 1.9 kW.

The NH_3/H_2 flame can be stabilized for a relatively wide range of equivalence ratios for all fuel mixtures. In general, the lean limit of equivalence ratio increases with the increase of ammonia in the fuel mixture, while the rich limit has an increase until $x_{NH_3} = 0.7$ and decreases gradually with the increase of ammonia.

The decrease observed for $x_{NH_3} < 0.7$, which are the conditions with higher content of H_2, can be explained due to the high diffusivity and reactivity of the hydrogen which causes flashback of the flame for lower values of x_{NH_3}. The decrease for $x_{NH_3} > 0.7$ is caused by the lower flame speed of the fuel mixture due to higher content of NH_3 and at the maximum ϕ, the flame simply extinguishes.

This difference of behaviour observed for the mechanism controlling the maximum equivalence ratio was also registered by Khateeb et al. [28]. As it can be seen in Figure 1.8, the author also observed flashback until a certain point ($x_{NH_3} = 0.5$) and after that point the maximum ϕ also had a considerable increase occurring rich blow out. The value of x_{NH_3} which corresponds to the behaviour change is higher for this work, when compared to the referred work, mainly because in this work the fuel blend is NH_3+H_2

while in the work of Khateeb et al. [28] it is NH_3+CH_4. This difference in the fuel blends makes the one with hydrogen more reactive while the molar fraction of NH_3 is decreased, occurring flashback phenomena for blends with more quantity of NH_3 when comparing with blends of NH_3+CH4. Also, the differences in the burners features (for example the swirl intensity) could help to give the different results.

Continuing to observe the Figure 4.2, both limits increase with the increase of the thermal input, but while for the lean limit, the difference between values is not that significant, for the maximum equivalence ratio limit, the values have a considerable increase. This observation shows the difficulty of burning these mixtures with less air when using lower thermal input probably due to the low velocities in the overall flow (fuel+air).

When using 1.9 kW as thermal input, as it can be seen in Figure 4.2, stable flames for $x_{NH_3} > 0.9$ were possible to achieve, however, with much narrow range as for the other conditions. Even being possible to have a pure ammonia flame, the operational range is still too low which means that more improvements are needed in the combustor. The increase of thermal power could widen the stable region for pure ammonia.

4.2. Test Conditions

After getting the stability map for all the thermal inputs previously defined, it was decided to move on with the maximum thermal input (1.9 kW) not only because it has a wider range of stability but also because it is more close to the thermal inputs with practical application, therefore more interesting to be studied.

It was in the scope of this work, while operating in lean regime, to assess the influence of the equivalence ratio and the ammonia molar fraction in the fuel on temperature and emissions. To do that, some flame conditions were selected, numbered as flame 1 to 5 and are represented as stars in Figure 4.3. The flames are also discriminated in Table 4.1 showing the conditions studied as well as the fuel and air flow rates. The injection velocity is also indicated, which refers in this case to the velocity of the partial mixture of reactants when entering the quartz tube, i.e. when passing through the gap between the outer tube internal wall (ϕ= 38 mm) and the bluff-body (ϕ= 34 mm).

Table 4.1- Studied flame condition and their flow rates and velocities.

Flame	x_{NH_3}	**ϕ**	**Air flow rate (L/min)**	**H_2 flow rate (L/min)**	**NH_3 flow rate (L/min)**	**Injection velocity (m/s)**
1	0.7	0.8	37.27	2.78	6.49	3.43
2	0.8	0.8	37.70	1.81	7.24	3.44
3	0.9	0.7	43.55	0.88	7.95	3.86
4	0.9	0.8	38.11	0.88	7.95	3.46
5	0.9	0.9	33.87	0.88	7.95	3.15

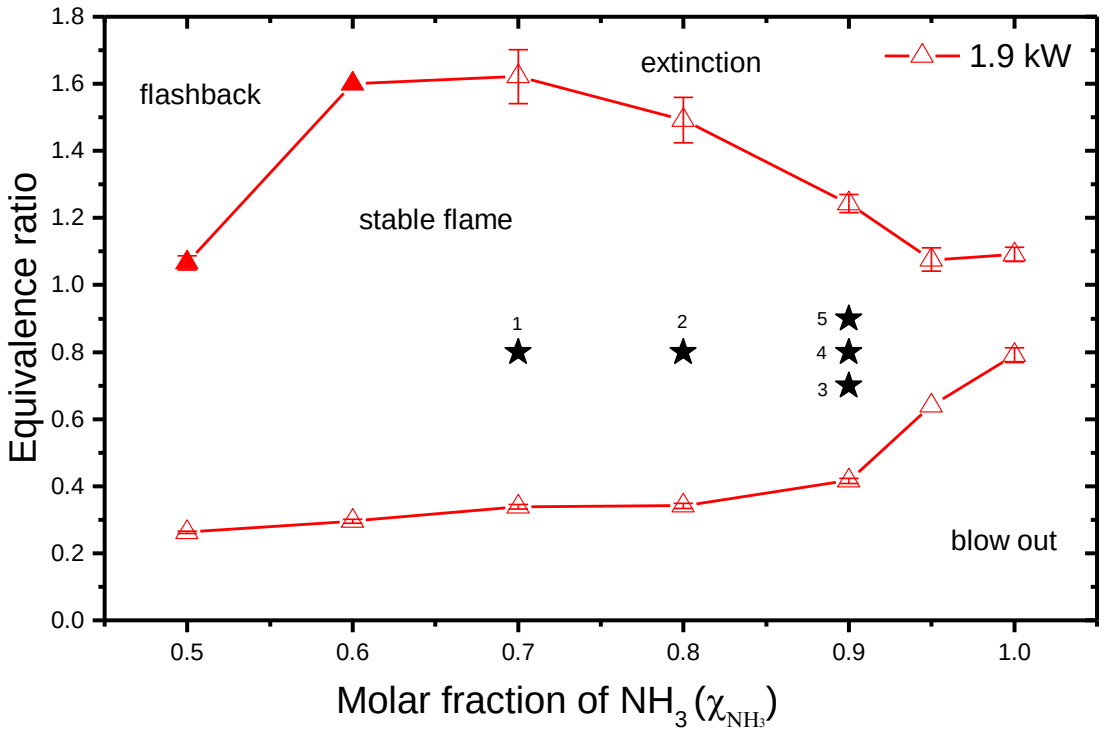

Figure 4.3 - Stability diagram for 1.9kW. Stars represent the flame conditions studied for all the measurements listed in Table 4.1.

This work has also the objective of providing data inside of the combustor giving a kind of a “map” of temperatures and emissions within the flame and the quartz tube. Each measurement was taken for an “r” and “z” couple, being “r” the radial distance from the combustor center and “z” an axial distance from the bluff-body level (Figure 3.9). “r” values were varied from 0 to 30 mm with 5 mm of increment. The “z” values were not varied linearly and are z= 30, 50, 70, 90, 120, 150, 200, 250 and 300 mm. The reason for that was the idea of being more interesting having a finer grid near the bluff-body and the flame zone than in the end of the quartz tube, where it was expected that the measured values were more uniform and the variances were smaller.

4.3. Temperatures

The first tests performed after choosing the working conditions, Table 4.1, were the temperature measurements. The procedure for these tests is described in 3.2.3. Differently of what has been said in the last section (4.2), for the temperature it was possible to take measurements for z = 10 mm without jeopardizing the flame stability while for NO_x this was not verified. However, the measuring zone was

considered to be the one represented in **Erro! A origem da referência não foi encontrada.** a) for being the one common for all tests.

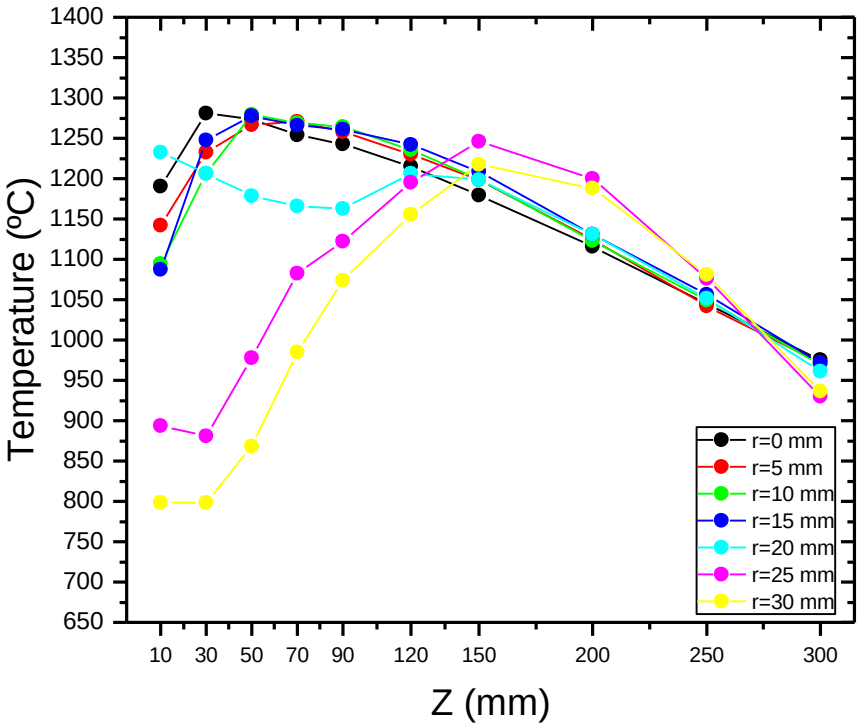

Figure 4.4 - Temperature distribution along the axial axis (z) for the studied radiuses (r). The condition represented is the flame 4 (x_{NH_3} = 0.9 and ϕ = 0.8).

Figure 4.4 represents, for flame 4, the evolution of temperature along the axial axis (z) for all the radial positions (r) studied. This condition is the one common to the 2 variations made (Figure 4.3), the variation of the NH_3 molar fraction in the fuel (x_{NH_3}) and the variation of equivalence ratio (ϕ).

Looking to the figure, the temperature of the flame raises until z = 50/70 mm and decreases afterwards. Despite the decrease of the temperature seems almost linear, it can be observed that after z=120 the decrease is more significant. The results are consistent for all radial positions studied, except for r ≥ 20.

For r > 20 mm the profiles have a much different behaviour. The temperatures for these radiuses are quite lower for z ≤ 90 mm since these points belong to a region outside of the recirculation zone where there is no combustion. However, from z= 120 mm the temperatures are closer to the ones of r < 20 mm mainly due to diffusion and heat transfer phenomena until an equilibrium is reached close to the exit (z = 300 mm), where the temperatures are similar for all the radial positions.

For 15 < r < 20 mm there is a change in the behaviour of the temperature profiles. In all the cases, the temperature profile for r = 20 mm has a unique tendency between the other radiuses and has a different tendency also between the flames. This could happen because in this zone, as schematized in **Erro! A origem da referência não foi encontrada.** b), is where the injection of the reactants is taking place. Therefore, depending on the height and the flame condition, in this radius, for z < 120 mm, we can have

the thermocouple placed in a zone outside the recirculation zone where combustion is not happening yet or is starting to occur. Also, in theory this is the region where there are higher velocities and there is more O2 concentration which contribute to have lower temperatures.

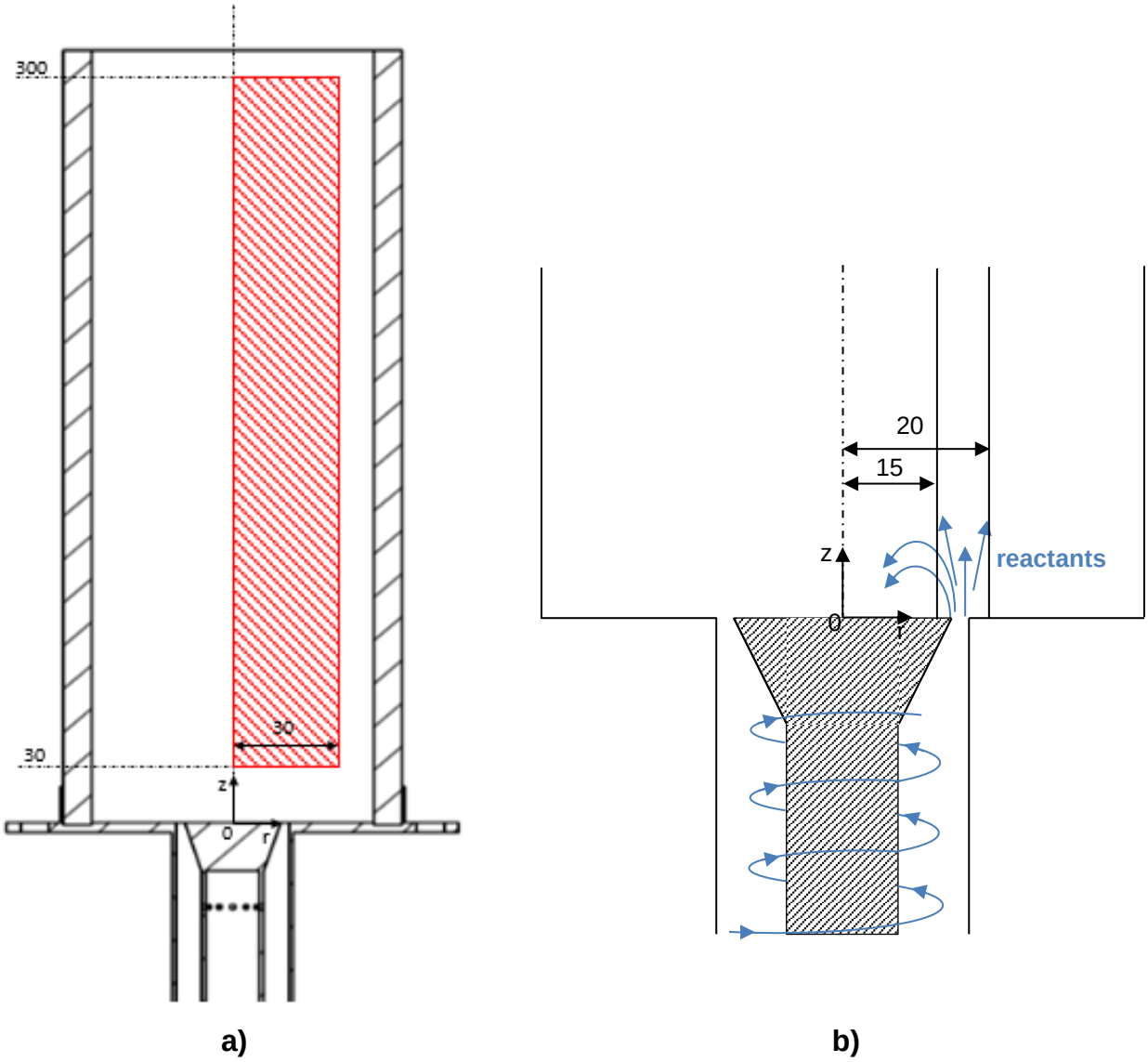

Figure 4.5 - a) Representation of measuring zone (dash filled red rectangle), comprised within 30 < z < 300 mm and 0 r < 30 mm. b) Schematic of the injection zone (15 < r < 20 mm).

Erro! A origem da referência não foi encontrada. represents the graph with the variation, for each z, o f the temperature along the radius with a comparison between the equivalence ratios used. In Figure 4.6 we can see that the temperature increases with the increase of the equivalence ratio. This happens because while we are decreasing the equivalence ratio, we are subsequently increasing the air used for combustion, which means that there is more O_2 and N_2 during and after combustion, leading to reduced temperatures. However, for most of the heights, the temperatures of ϕ=0.9 and ϕ=0.8 are closer when

comparing to ϕ=0.7. This could mean that for ϕ = 0.7 either the temperatures created are lower and the cooling is more intense for this condition.

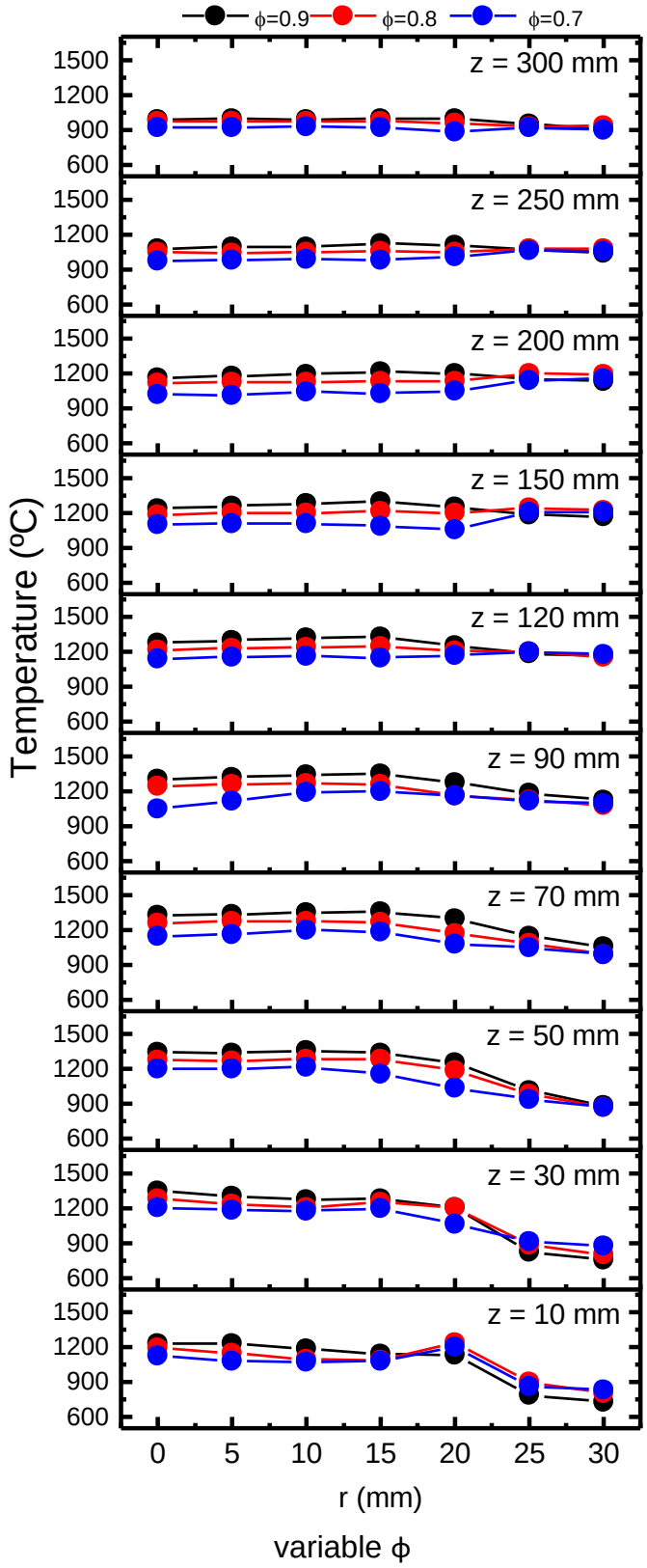

Figure 4.6 - Temperatures along the r for each z. The curves represent the equivalence ratio variation at a fixed NH_3 molar fraction ($x_{NH_3} = 0.9$).

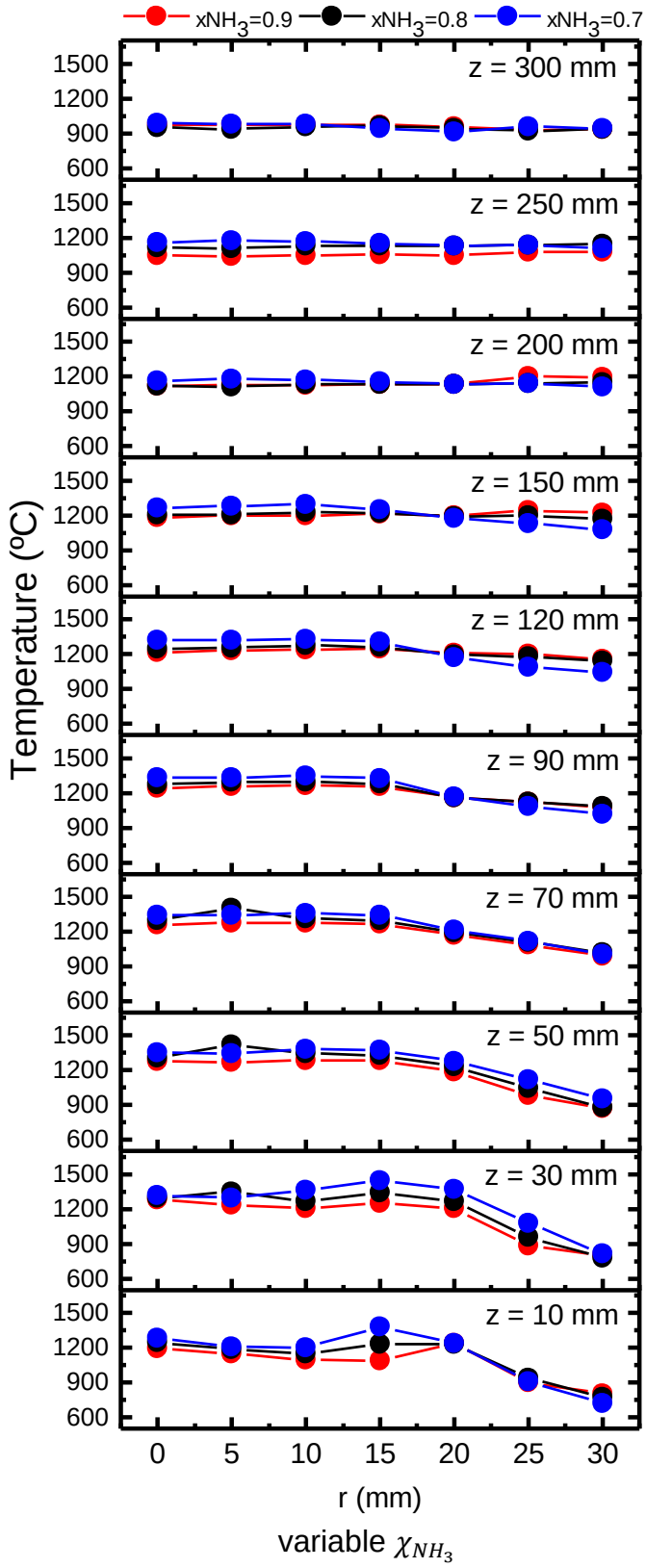

Figure 4.7 - Temperatures along the r for each z. The curves represent the variation of the NH_3 molar fraction in the fuel for a fixed equivalence ratio (ϕ=0.8).

Figure 4.7 represents the graph with the variation, for each z, of the temperature along the radius with a comparison between the NH_3 molar fractions used. Observing the graph, the temperatures are more similar between the flame conditions than for Figure 4.6, only having more different values between the curves for z's closer to the bluff body. This is probably because we are using the same equivalence ratio, which gives a similar air flow rate and a similar afterburn concentration of O_2 throughout the combustor. In general, the temperatures increase with the decrease of the NH_3 molar fraction in the fuel. This was expectable since in this way we are increasing the H_2 molar fraction, which is more reactive and has a higher flame temperature than NH_3, therefore increasing the flame temperature of the mixture.

It is visible in both graphs, as already mentioned, that for r > 20 mm and z < 120 mm, the temperatures are increasing with the height. It is also observable that the temperatures vary along the radius, being the more notable differences for lower z's, where the combustion occurs, and the recirculation is stronger. For the most conditions, for z > 120 mm the temperature profiles along the radius starts to be constant.

With the values obtained through the temperature measurements and resourcing to a computer data analysis software (Origin) to make some interpolations, we obtain an approximation of the temperature distribution inside the combustor in the measuring zone (**Erro! A origem da referência não foi encontrada.** a)).

Figure 4.8 and Figure 4.9 it is represent the results obtained from the same software for temperatures distribution. Here it can be seen the higher values are in the recirculation zone while the lower values, as concluded before, are in the zone outside the recirculation and at low heights. Also, it can be seen the reduction of temperature along the axial axis (z) and the more uniform temperature distribution across the radius (r) near the exit of the combustor. In Figure 4.8 we have the variation of the NH3 molar fraction in the fuel represented. As observed in Figure 4.7, the temperatures decrease with the increase of the NH3 molar fraction. Knowing that the maximum temperatures are for the recirculation zone, the figure shows that we have a stronger recirculation zone while we decrease the NH3 molar fraction, giving a more compact high temperature zone closer to the combustor axis. This is mainly due to the higher reactivity of the hydrogen which gives higher temperatures resulting in a more uneven distribution.

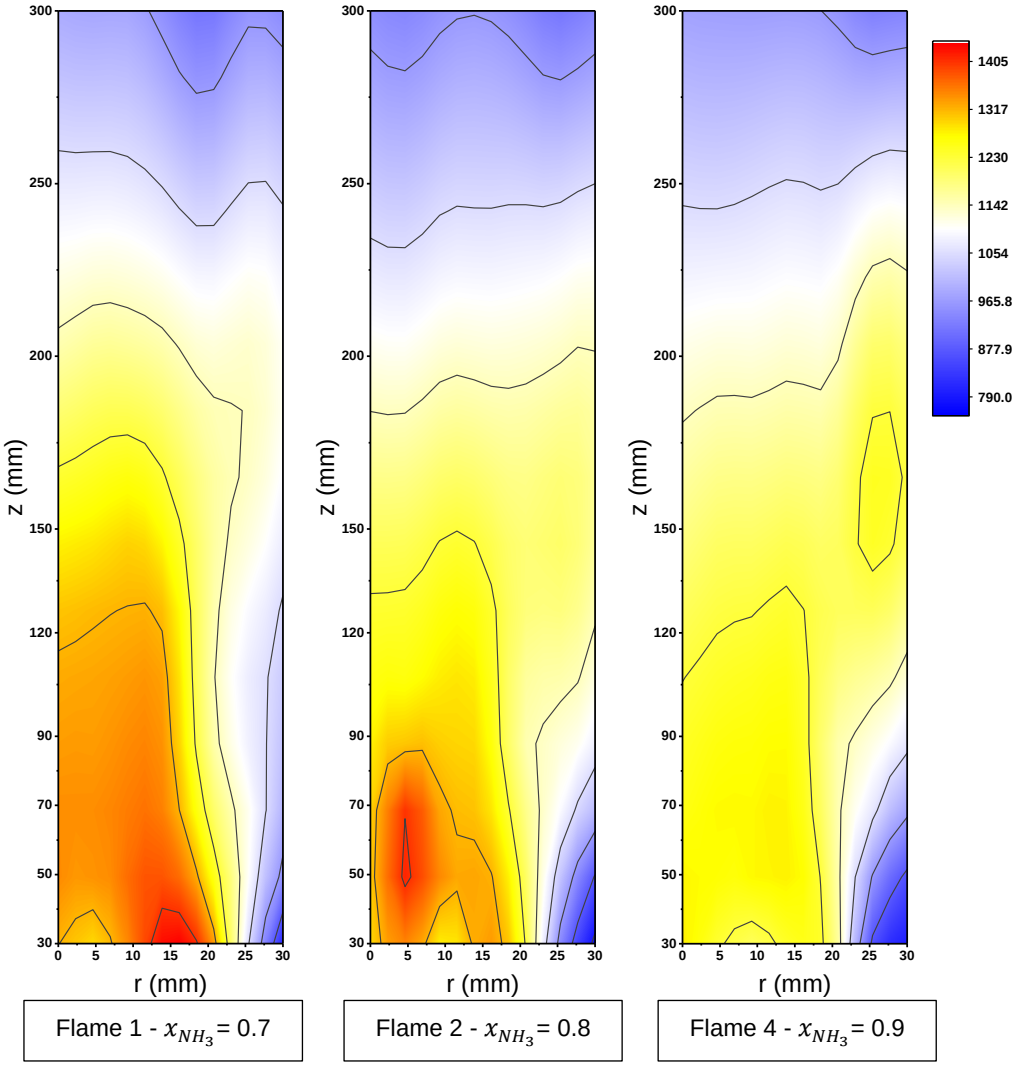

Figure 4.8 - Temperature distribution inside the combustor corresponding to the measuring zone (figure). Represented the flame conditions with the same equivalence ratio (ϕ=0.8).

In Figure 4.9 we have the variation of the equivalence ratio. As mentioned before, the temperatures increase while we are reaching stoichiometric conditions and the difference of values between each condition represented here is higher than for the variation of the NH_3 molar fraction (Figure 4.8). For flame 3 the temperatures are more spread not having a denser high temperature zone near the center as for the other flames. This could indicate that recirculation is weaker, and the recirculation zone is not that defined. This could be happening due the higher velocity of the reactants, because of the increase of the air used. Also, the increase of the air, will subsequently increase the intensity of the swirl which could interfere with the intensity of the recirculation caused by the bluff body giving lower temperatures and worse distribution.

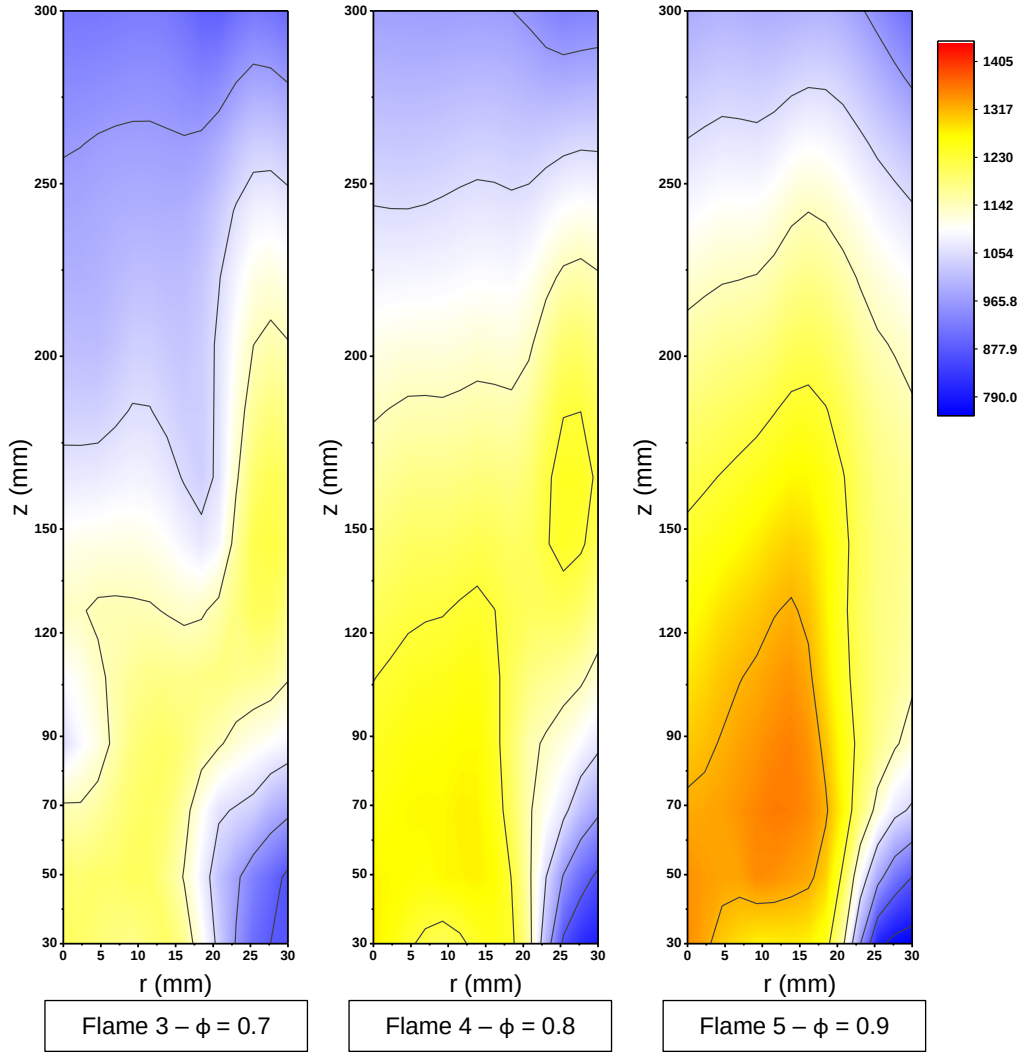

Figure 4.9 - Temperature distribution inside the combustor corresponding to the measuring zone (figure). Represented the flame conditions with the same NH_3 molar fraction in the fuel ($x_{NH_3} = 0.9$).

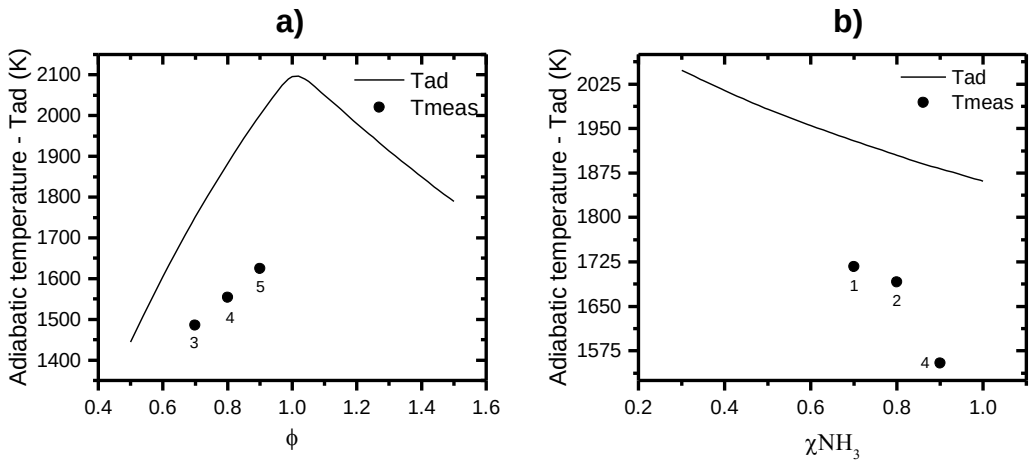

Figure 4.10 - Representation of the adiabatic temperature a) for different equivalence ratios (ϕ) at $x_{NH_3} = 0.9$ and b) for different NH_3 molar fractions in the fuel at ϕ = 0.8. The black dots are the maximum experimental measured temperatures for each flame condition. Tad stands for the adiabatic temperature and Tmeas stands for the measured temperature.

Figure 4.10 represents the calculation of the adiabatic flame temperatures for various ϕ at x_{NH_3} = 0.9 (a) and for various NH_3 molar fractions at ϕ = 0.8 (b). It is also represented the maximum temperatures recorded in the measurements to give an idea of the difference between the theoretical ideal flame temperature and the maximum actual measured. This difference will be directly correlated to heat losses throughout the combustor. Even without calculating the heat losses, it can be seen that the temperature differences are relatively high, which means that there are still high heat losses in this combustor, needing an improvement on this subject.

Table 4.2 - Maximum temperatures measured for the flame conditions (flame 1-5) and its coordinates. Tmax stands for the maximum temperature measures both in ºC and K. Tad stands for the calculated adiabatic temperature for each condition.

Flame	Tmax (ºC)	r (mm)	z (mm)	Tmax (K)	Tad (k)
1	1444	15	30	1717	1929
2	1418	5	50	1691	1905
3	1213	10	50	1486	1751
4	1281	0	30	1554	1882
5	1352	10	50	1625	2001

Table 4.2 shows the values and the coordinates where the temperatures measurements gave the higher values for all the flames. It is clear that for all flames the maximum measured temperature is inside the recirculation zone being the zone with higher temperature in Figure 4.8 and Figure 4.9 around these coordinates.

Temperature measurements were made also for negative radius, i.e. for 0 < r < 30 symmetrical to the ones showed before relatively to the combustor symmetry axis. These measurements intended to conclude about the symmetry of the flame, and the results for flame 4 are represented in Figure 4.11. There it can be observed that temperatures have little differences for symmetrical radiuses, having only considerably differences for few points. These observations are valid for all 5 flames where it could be concluded, giving the nature of the flow inside the combustor, that the flames have good symmetry. For both positive and negative radius, for each point, the temperatures were taken 3 times.

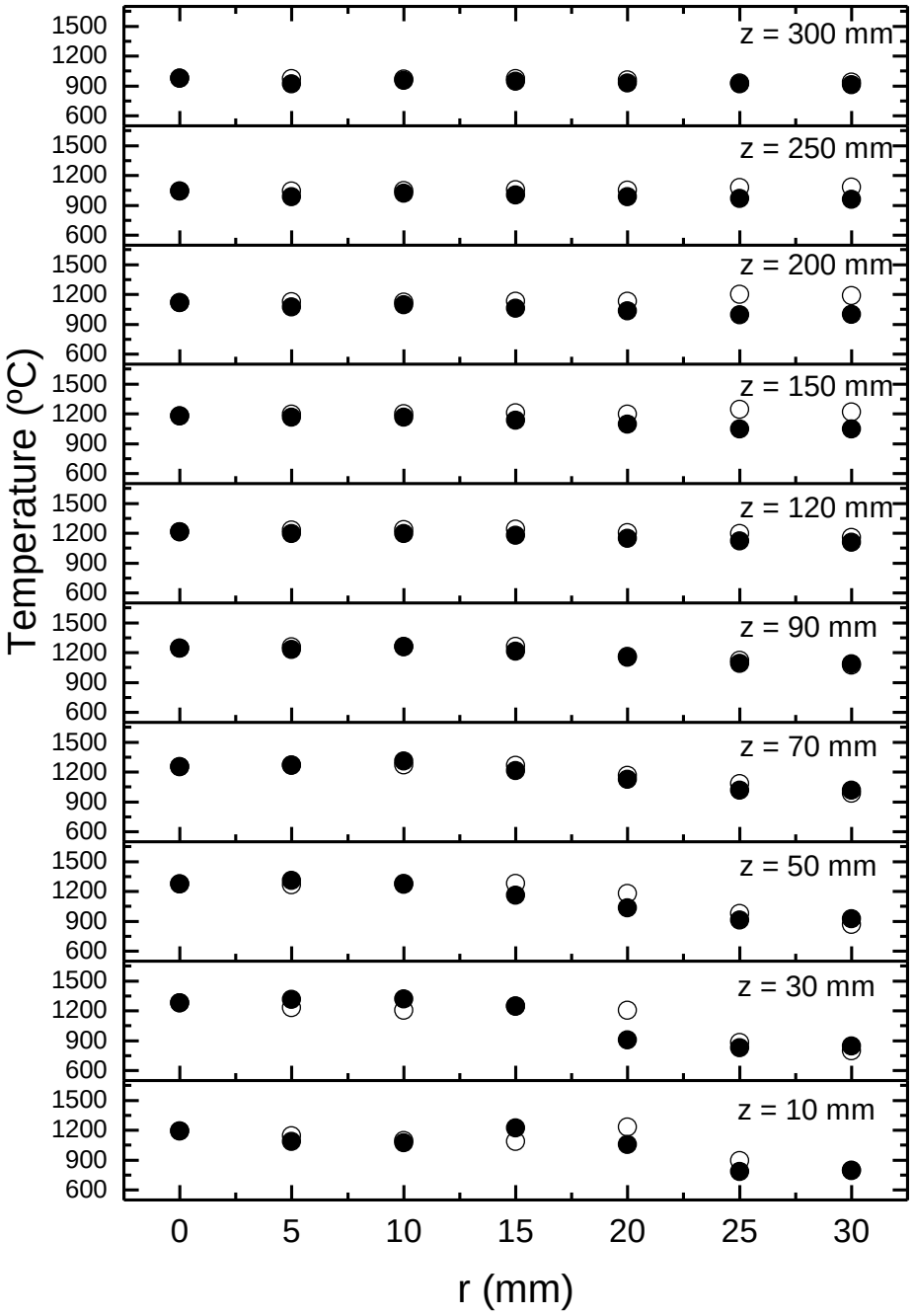

Figure 4.11 – Temperatures for symmetrical radial positions. Open dots represent the temperatures for what was considered to be the positive radius and the filled dots for the negative ones.

4.4. Gas species

4.4.1. Exhaust concentrations

In the case of the gas species, before taking measurements inside the combustor, it was measured for all the flames, the exhaust concentrations of NO_x and NH_3 as described in sections 3.2.4.1 and 3.2.4.2 respectively. These measurements were taken in the centreline of the combustor (r = 0 mm) at z = 300 mm and can be considered as the combustion emissions of this burner. In this way they were corrected for 13% of O_2 which is the standard value used for gas turbines and burners of this kind.

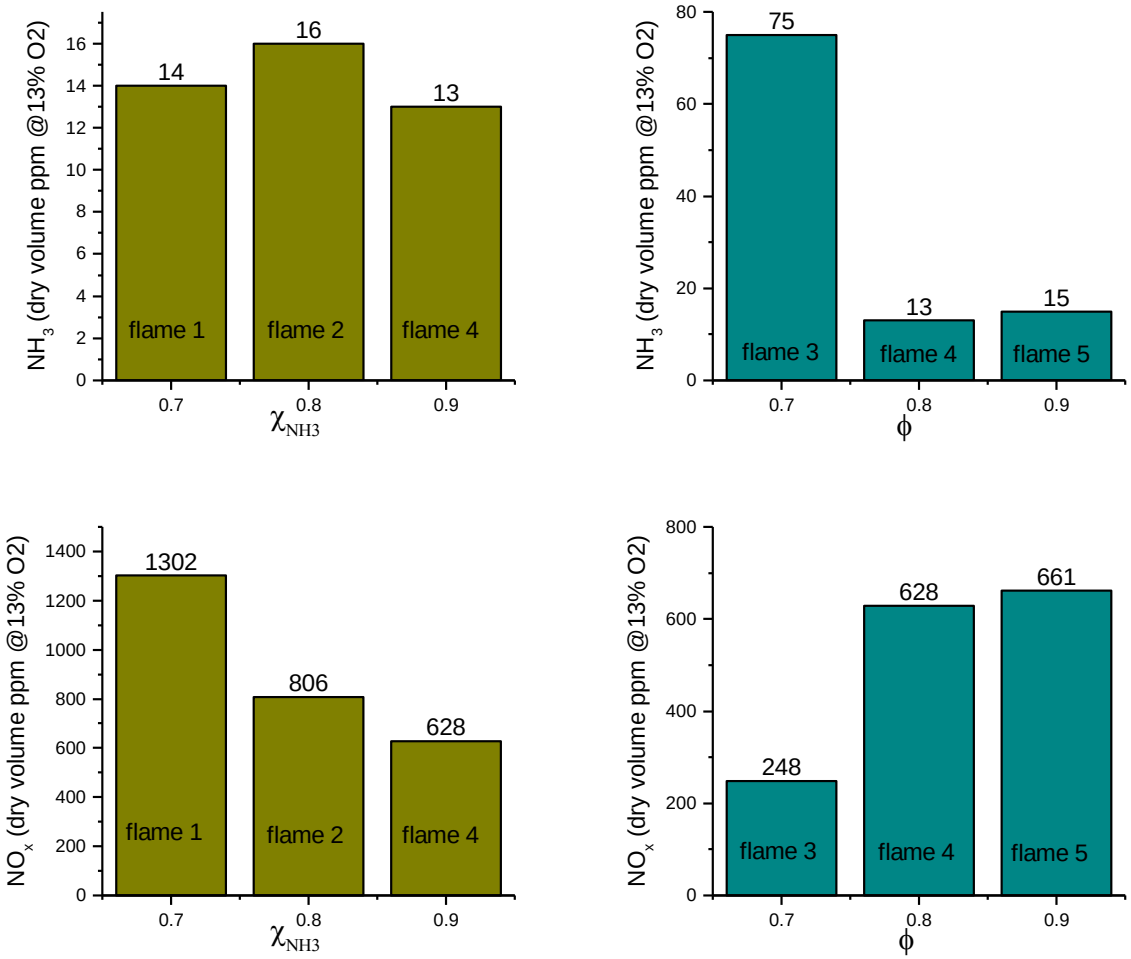

Figure 4.12 -Values of the corrected exhaust NO_x and NH_3 emissions taken at r = 0 mm and z = 300 mm. Green graphs represent the emissions for conditions with the same equivalence ratio (ϕ = 0.8) with x_{NH_3} variable. Blue graphs represent the emissions for conditions with the same NH_3 molar fraction ($x_{NH_3} = 0.9$) with ϕ variable.

Figure 4.12 represents the values of exhaust NOx and NH_3 for all flames. The information is represented by grouping the values with same equivalence ratio and same NH_3 molar fraction and dividing in NH_3 and NO_x emissions for better comparison. It can be seen that the emissions of NH_3 are low and close to each other, an exception made for flame 3, where it was recorded a considerably higher value. Focusing on NO_x emissions, they decrease while increasing the molar fraction of NH_3. When varying

the equivalence ratio, the NO_x emissions are similar for flame 4 and 5 while for flame 3 the value is relatively lower. Both the higher NH_3 emissions and lower NO_x for flame 3 can be an indicator of poorer NH_3 conversion or incomplete combustion for this condition.

4.4.2. Concentration inside the combustor

The last measurements within the scope of this work were the species, more specifically NO_x and O_2, inside the combustor, in the same measuring zone represented in **Erro! A origem da referência não foi encontrada.** a). To accomplish that, the procedure described in 3.2.4.1. was followed.

Figure 4.13 shows the results of this type of measurements once again for flame 4. For each height (z) it is represented the curves of O_2 and NO_x variation along the radius as well the temperature variation.

It is easily observed that, as it happened for the temperatures, for r > 20 mm and z < 120 mm the values of NO_x are much lower than for the other points, being some of them close to zero. This is a reasonable result since in this region we do not have combustion and the temperatures are not high enough to produce NO_x. After z = 120 mm the NO_x for r > 20 mm starts to increase and it is practically constant across the radius near the combustor exit.

Still regarding the NO_x, the higher values were recorded for what we considered to be the recirculation zone, r < 20 mm and z < 120 mm, which is a zone with higher temperatures and higher concentration of combustion products, in this case fuel NO_x. The concentration of NO_x increased while we get closer to the bluff body and the center of the combustor. Again, after z = 120 mm the NO_x differences between the center and the other radiuses starts to decrease being almost constant at the exit.

The decrease of NO_x concentration across the axial axis (z) for r < 20 mm could be explained by species diffusion caused by the flow, however, it may not be the only mechanism occurring there. For z > 70 mm, in theory, SNCR could be taking place where some ammonia that had not been consumed in combustion may be being consumed in this region to reduce NO_x since the temperatures are in possible values for this phenomenon to happen.

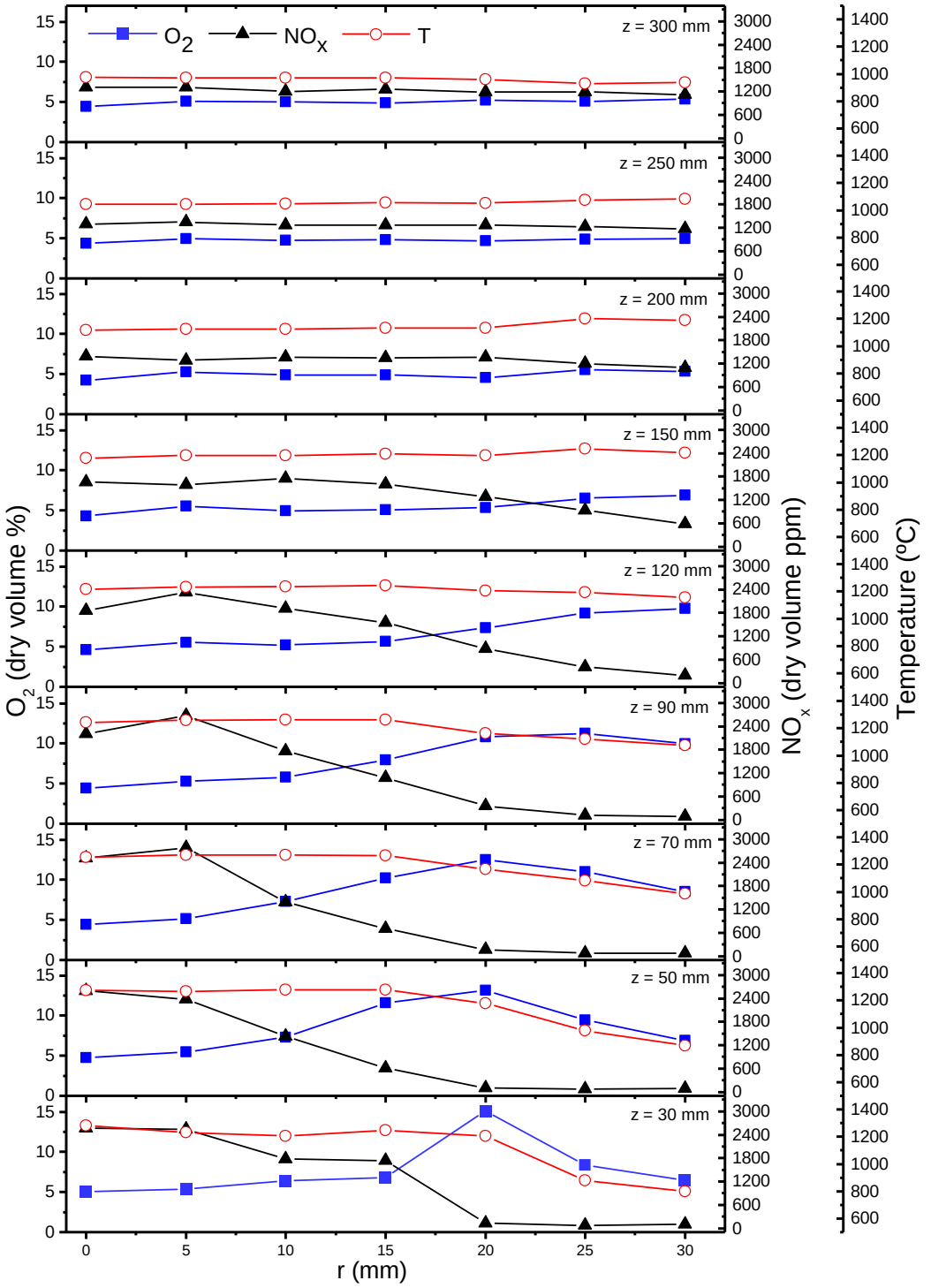

Figure 4.13 – Temperature, NO_x and O_2 concentrations along the radius for all heights (z) studied. This graph represents the results for flame 4 ($x_{NH_3} = 0.9$ and $\phi = 0.8$).

Other observations we can make is about the evolution across the radius of the O_2 concentration. As observed for the NO_x concentrations, for z > 120 mm the O_2 concentration tends to stabilize across the radius becoming relatively constant.

For z < 120 mm we can notice 3 different behaviors. For r < 20 mm the values of O_2 remain low, slightly increasing across the radius. As mentioned, this region corresponds to the recirculation zone, therefore

it was expected that the O_2 concentration was low because it is a zone where, in theory, there are more concentration of combustion products and less concentration of O_2 which was consumed during combustion.

For r = 20 mm, there is a peak of the O_2. As mentioned before and represented in **Erro! A origem da referência não foi encontrada.** b), this radius is near the injection zone of the reactants which mean that, depending on the condition and the height, the maximum O_2 is recorded for this radius because the combustion is not happening yet in this region making the O_2 injected in there not yet consumed.

For r > 20 mm, O_2 concentration decreases again, being slightly higher than the values for r < 20 mm. This could happen since this is a zone outside the recirculation zone, where there is no combustion and there is some non-consumed O_2 from the reactants present there.

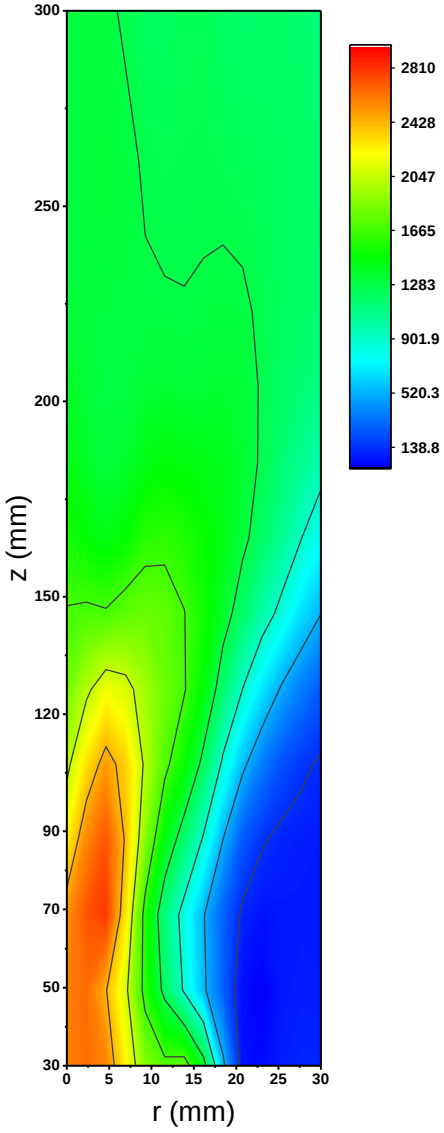

Figure 4.14 – NO_x distribution inside the combustor in the measuring zone (**Erro! A origem da referência não foi encontrada.** a)) for flame 4 ($x_{NH_3} = 0.9$ and $\phi = 0.8$).

Using the same software as for the temperatures, the NO_x concentration distribution throughout the measuring zone was obtained (Figure 4.14). Here it can be seen clearly the higher concentration near the centre of the combustor for z < 120 mm and the lower concentration region, also for z < 120 mm, but far from the centre, outside the recirculation zone (r ≥ 20 mm). It is also clear that, as already mentioned, the concentration of NO_x near the exit is reasonably constant along the radius.

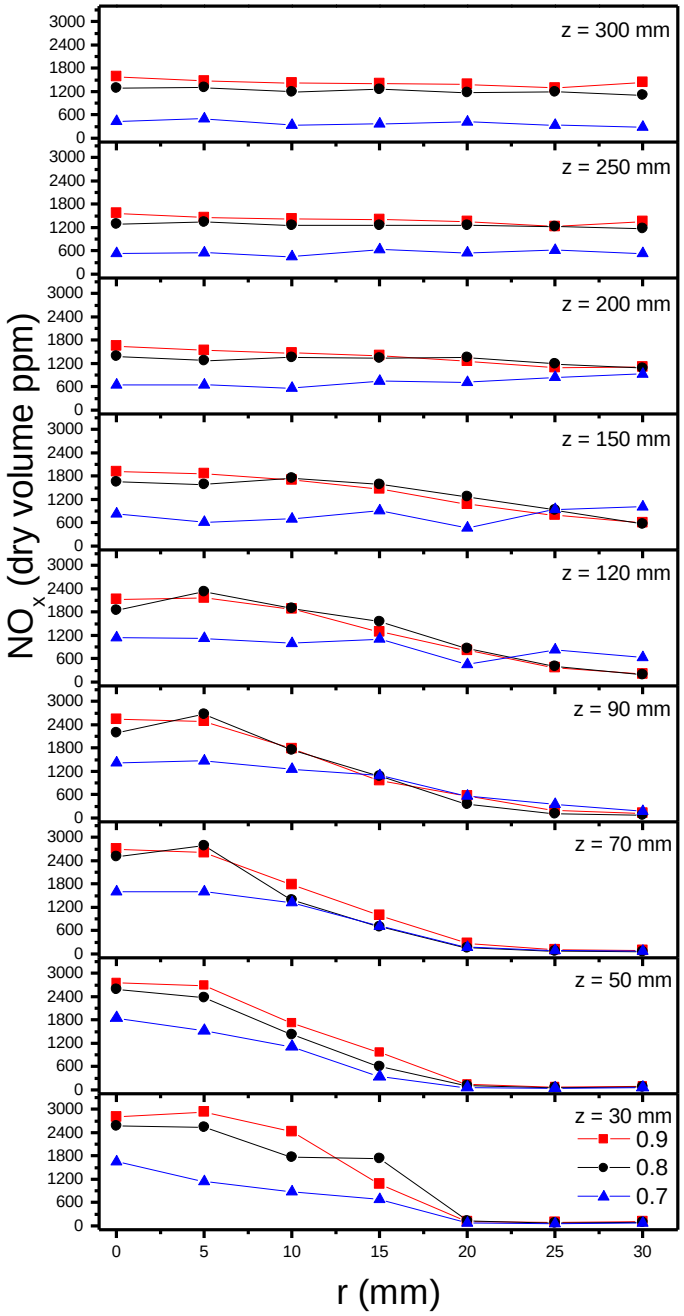

Figure 4.15 – NO_x profiles along the radius (r) for all heights (z) of the conditions with the same NH_3 molar fraction ($x_{NH_3} = 0.9$). blue line corresponds to flame 3, black line to flame 4 and redline to flame 5.

Figure 4.15 shows the profiles of NO_x concentration along the radius, for each z, of the flames with the same NH_3 molar fraction ($x_{NH_3} = 0.9$), therefore being a representation of the effect of the equivalence ratio on the NO_x concentrations.

Here it can be seen that the profile tendencies for ϕ = 0.8 and ϕ = 0.9 are similar being the values pretty close between them, on overall higher for ϕ = 0.9, verifying only a greater difference for the zone of r < 20 mm and z < 70 mm.

Looking at the profiles for ϕ = 0.7 (blue), the tendency for lower z's is much different from the other 2 conditions being the values for all heights are considerably lower. This fact could indicate that, for some reason, incomplete combustion could be happening which would reduce the amount of NO_x production during the combustion process. On the other hand, an incomplete combustion, in theory, would lead to higher amount of unburned fuel in the products which could be the same to say higher amount of NH_3. This theoretical increase of NH_3 presence in the products could improve the SNCR intensity reducing the already lower concentration of NO_x.

The lower values of NO_x recorded for flame 3 and the slightly higher exhaust NH_3 emissions for this flame (Figure 4.12) both contribute to the theory of the incomplete combustion for this condition.

Figure 4.16 has the same profiles as Figure 4.15 but for O_2 concentrations. Here the tendencies are more consistent than for NO_x being similar for all the heights. It is noticeable that the peak of O_2 happened at r = 20 mm for all the conditions and that, globally, the O_2 concentration increased with the decrease of the equivalence ratio. This increase was expectable since while reducing the equivalence ratio, we are increasing the excess air used in combustion giving higher concentration of O_2 in the products.

Table 4.3 – Values of the average measured O_2 concentration at the exit (z = 300 mm) and the theoretical calculated O_2 concentration.

Flame	Measured O_2 (%)	Theoretical O_2 (%)
3	7.05	6.55
4	5.01	4.32
5	3.14	2.1

Table 4.3 shows a comparison between the O_2 recorded during measurements and the O_2 expected after combustion. For the measured O_2 it was considered the average of the O_2 values across all the radiuses for z = 300 mm and the theoretical O_2 were obtained using equilibrium equations at adiabatic temperature. The difference between the 2 values are not that different for all the flames and even for flame 3, where it was speculated to have incomplete conversion of NH_3, the O_2 difference is the smallest which means that O_2 could be being consumed for secondary reactions.

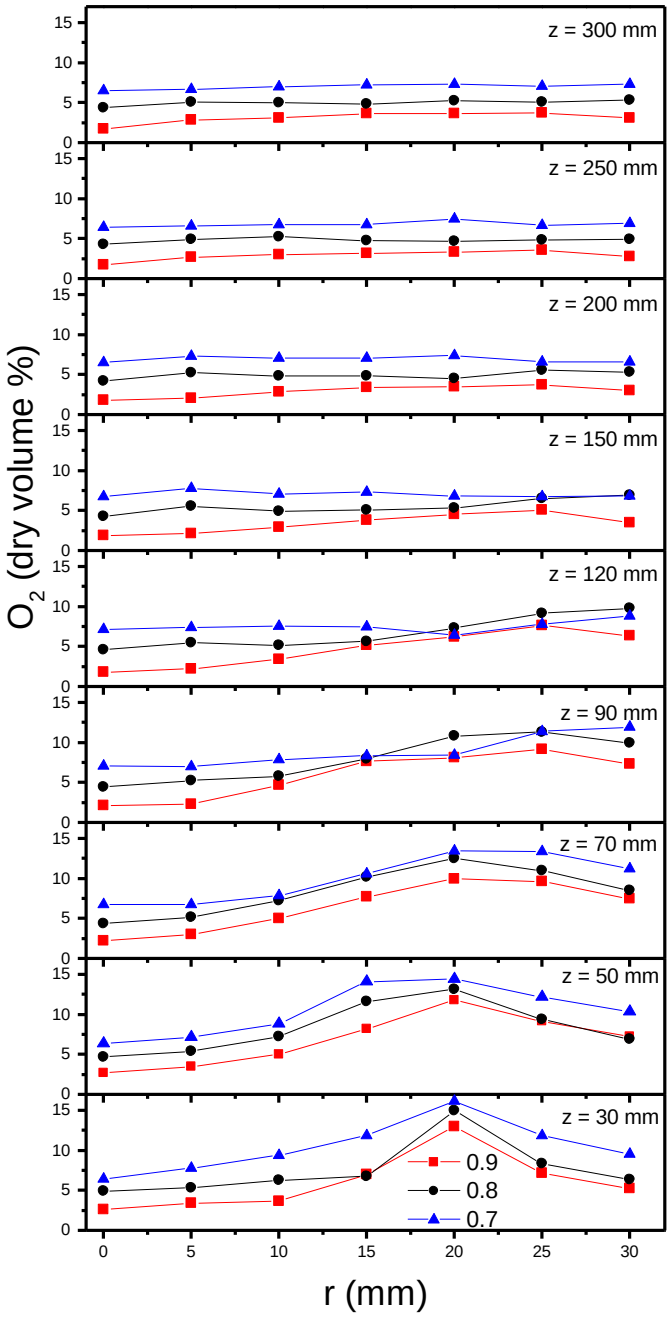

Figure 4.16 – O_2 profiles along the radius (r) for all heights (z) of the conditions with the same NH_3 molar fraction ($x_{NH_3} = 0.9$). blue line corresponds to flame 3, black line to flame 4 and redline to flame 5.

The same comparison can be made for the flames with same equivalence ratio (ϕ) and different NH_3 molar fraction in the fuel (x_{NH_3}). In this case the equivalence ratio was fixed at ϕ = 0.8 and the NH_3 molar fraction was varied from 0.7 to 0.9 corresponding to flames 1, 2 and 4 as shown in Table 4.1.

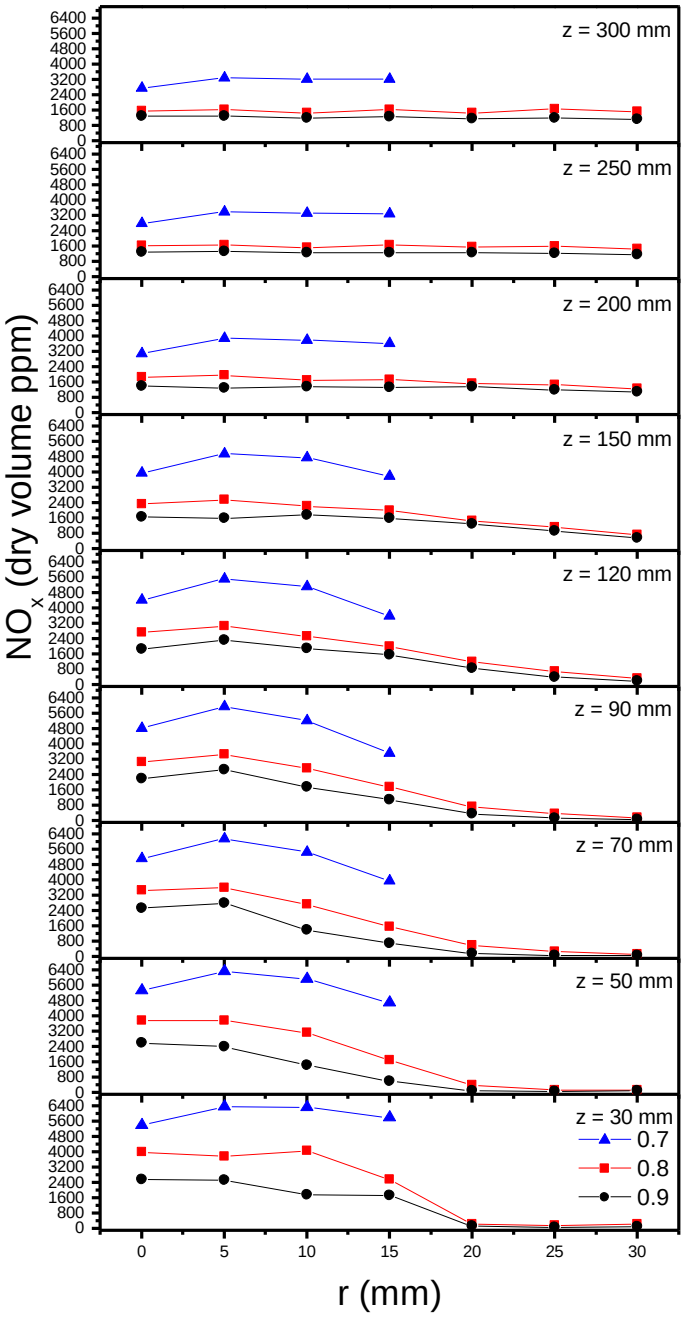

Figure 4.17 - NO_x profiles along the radius (r) for all heights (z) of the conditions with the same equivalence ratio (ϕ = 0.8). Blue line corresponds to flame 1, black line to flame 4 and red line to flame 2.

Figure 4.17 shows the NO_x concentration profiles along radius for the flames with the same equivalence ratio, varying the NH_3 molar fraction in the fuel (x_{NH_3}) between each curve. This representation is a way to assess the effect of x_{NH_3} in the NO_x concentration.

It is worth mentioning that for flame 1 (blue line) the curves are incomplete because it was not possible to finish the measurements due to malfunctions of the analysers which were not fixed in time for this work.

Comparing the flames 2 (red line) and 4 (black line), it could be seen that the tendencies are very similar to each other on every height (z), being the values for flame 2 always higher than flame 4. However, for the recirculation zone (r < 20 mm and z < 70 mm), the difference between the values is considerably higher than in the other regions. For z > 70 mm the difference starts to reduce, still being noticeable, and for z > 200 mm this difference is minimum. For r > 20 mm the NO_x concentrations are practically equal for all heights.

In Figure 4.17, despite being incomplete, it is represented the values measured for flame 1. The values of NO_x concentration are much higher for all measured points than for the other flames, being the difference between flame 1 and 2 also much higher than between flame 2 and 4.

This increase on NO_x concentration with the decrease of NH_3 molar fraction in the fuel (x_{NH_3}) observed here is directly correlated with the fact that while decreasing the quantity of NH_3, in this dual fuel approach adopted for this work, it is increased the quantity of H_2 present in combustion. The increase of H_2 concentration in the fuel, as said before, makes the mixture more reactive due to the H_2 higher reactivity, higher flame speed and higher flame temperature than NH_3. This increase in the mixture reactivity will increase the generation of OH and O radicals due to the H_2 oxidation pathways. These radicals are fundamental for the HNO pathway, which is the most important on the NO formation [34, 35]. In this way the increase of H_2 in the fuel mixture will lead to higher intensity of the chemistry behind NO_x formation increasing the values of NO_x concentration.

Figure 4.18 represents the O_2 profiles for the same flames as in Figure 4.17. As expected, since they have the same equivalence ratio, the O_2 concentration follows the same tendency and the values are close to each other. This tendency is similar to the one verified in Figure 4.16 having also a peak in r = 20 mm due the same reasons explained before.

On the overall, the developed burner worked well for the proposed study showing good stable operation conditions. The flame was stable during all the extensive measurements done in the scope of this work. The burner revealed to work well with high amounts of NH_3 in the fuel mixture and with promising emissions for some of the conditions. The temperatures recorded at the exit of the burner were also relatively high, in a range between 900-1000 ºC. All that gives promising perspectives for the future use of this burner to continue exploring the use of NH_3 combustion.

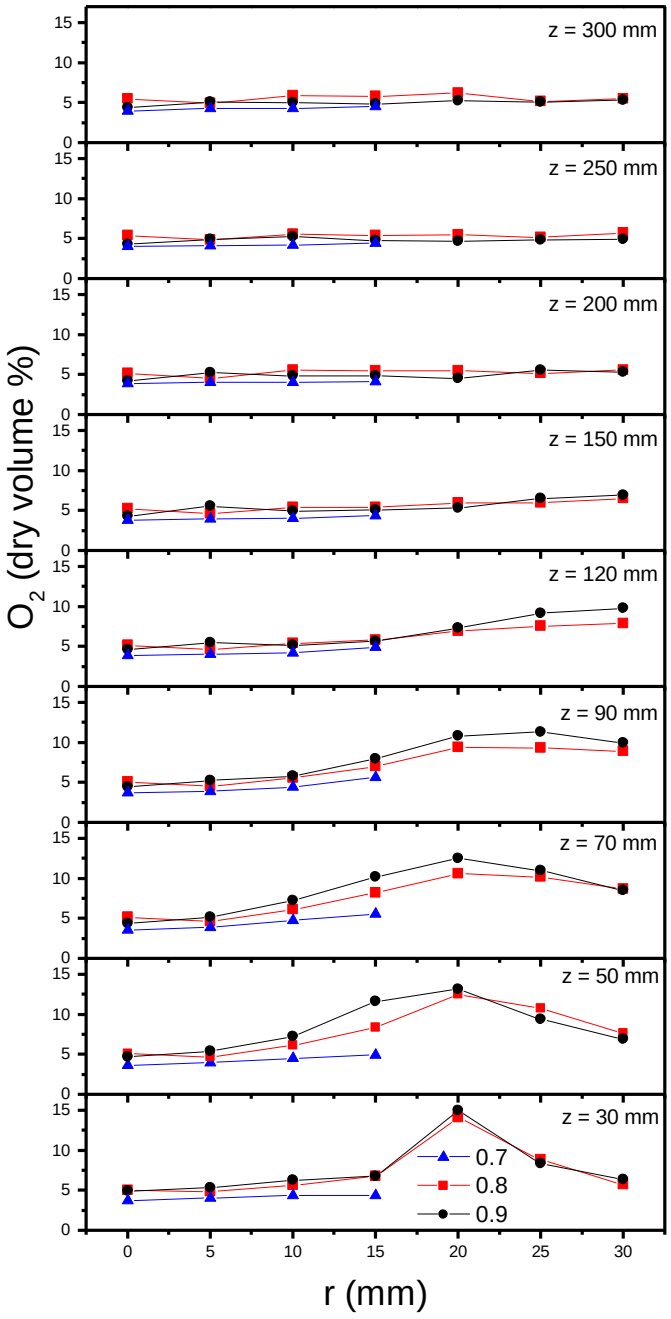

Figure 4.18 – O_2 profiles along the radius (r) for all heights (z) of the conditions with the same equivalence ratio (ϕ = 0.8). Blue line corresponds to flame 1, black line to flame 4 and red line to flame 2.

5 Conclusions

5.1. Summary

The work proposed in this thesis was to test a newly developed burner for our laboratory that combines some combustion techniques to burn ammonia in a more stable way. After that it was intended to do some tests and measurements to characterize the burner and assess its operability, also giving experimental data to compare with numerical simulation and help to improve the models used for that purpose.

To do so, after the burner design, development and manufacture, tests varying the air supply were made to assess the stability limits for NH_3 molar fractions (x_{NH_3}) varying from 0.5 to 1 with 0.1 increments. These tests were made for 3 different thermal inputs and after having the stability diagram for all, it was decided to proceed to the measurements with the highest thermal input, 1.9 kW.

The next step was to take measurements of temperatures, exhaust emissions and NO_x and O_2 concentrations inside the combustor. The flame conditions for these measurements were chosen aiming the assess the effect of varying the equivalence (φ) ratio and the effect of varying the NH_3 molar fraction of the fuel (x_{NH_3}), giving 5 flame conditions.

Table 5.1 – Investigated fame conditions.

Flame	x_{NH_3}	φ
1	0.7	0.8
2	0.8	0.8
3	0.9	0.7
4	0.9	0.8
5	0.9	0.9

The temperature, the NO_x and O_2 measurements were taken for all the 5 flames and, as they also intend to give data in the inside of the combustor, they were taken for r between 0 and 30 mm and z between 30 and 300 mm, which was called as the measuring zone. The exhaust emissions measurements were taken at r = 0 mm and z = 300 mm for NO_x and NH_3 emissions.

The results obtained with this work give an extensive data of the combustor's inside which will help to complement and improve the numerical models used for modelling this burner and the ones of its kind.

5.2. Main conclusions

From the present work, the main conclusions can be resumed as follows:

- During stability tests, it was found a relatively wide operational range of the combustor for all NH_3 molar fractions in the fuel and for all thermal inputs. It was also observed an increasing on the stability region with the increase of the thermal input, especially due to the increase of the rich stability limit. For all thermal inputs, the highest equivalence ratio was reached at $x_{NH_3} = 0.7$. At the rich stability limit, flashback occurred for $x_{NH_3} < 0.7$ and for $x_{NH_3} > 0.7$ the flame simply extinguishes. Pure ammonia flame was only achieved for the highest thermal input, 1.9 kW.

- Concerning the temperatures, the maximum ones were recorded for z ≤ 50 mm and r ≤ 15 mm in all the flames, which is inside the recirculation zone. Temperature profiles along the axis (z) were consistent for r ≤ 15 mm and for r ≥ 25 mm but for r = 20 mm the profile is highly influenced by the reactants injection. Temperature decreases with the decrease of the equivalence ratio, mainly due the higher concentration of O_2 and N_2 during combustion, and increases with the decrease of the x_{NH_3} due to the higher presence of H_2 which is more reactive and has higher flame temperature than NH_3. The temperature at the exit of the combustor seems high enough for implementation of second stage combustion, however, there were still high thermal losses, which means that the insulation of the combustor has room for improvement.

- Exhaust measurements showed that exhaust NO_x increase with the decrease of the x_{NH_3}. While varying the equivalence ratio, exhaust NO_x was relatively equal exception made for flame 3 ($x_{NH_3} = 0.9$ and ϕ = 0.7), which gave lower value. Exhaust ammonia was found low, except for flame 3, which gave a relatively high value. For flame 1 it was recorded excessively high NO_x emissions.

- Focusing on the inside of the combustor, O_2 concentrations were similar while varying x_{NH_3} and increased with the decrease of ϕ, having all the flames a peak of O_2 at r = 20 mm. NOx concentrations were higher inside the recirculation zone and for lower z's. There was a decrease of NO_x concentrations along the axis (z) due to the species diffusion and possibly to SNCR mechanism, since the temperatures along the combustor are in possible values for that to happen. NO_x concentrations decrease with the decrease of the equivalence ratio however, they are close for ϕ = 0.9 and 0.8 and considerably lower for ϕ = 0.7. Also, they increase with the decrease of x_{NH_3} due to the higher content of hydrogen, which prompts the generation of OH and O radicals that favours the NO formation.

- Considering the flame 3 results both for NH_3 exhaust emissions and the NO_x concentrations throughout the measuring zone, we can admit that incomplete combustion or fuel conversion is occurring for this condition.

5.3. Recommendations for future work

Reflecting over the findings of this work, the success of this burner to have stable flames with considerably high content of ammonia was proved. However, some improvements could be done, in terms of heat losses and perhaps in better equipment for reactants injection.

Using different techniques to measure species and temperatures would be of great interest because the ones used in this work are intrusive techniques which certainly will interfere with the flame. Comparing the measurements of the non-intrusive methods and our measurements will give the idea how the probe used influences the results obtained. Also, if some of these non-intrusive techniques can measure other species and radicals of interest, such as H_2, OH and NH_2, etc., it could give more insight of what is happening in the combustion zone.

It was clear that the stability increased while increasing the thermal input, which makes a natural next step to increase more the thermal input to observe the point where it changes, and the stability starts to decrease with further thermal input increase. Also, it would be interesting to increase the thermal input and see if it gives a wider stable region for pure ammonia.

For improving the NO_x emissions, the following investigation using this burner could be taking the flame conditions to the rich regime, contrary to the lean regime used in this work, which is known to have lower NO_x emission. However, it is needed to be aware of the emission of unburned fuels, which could be dangerous and threatening for humans.

Despite this, using a rich regime in this combustor, in theory could open the possibility of using a second stage of combustion after the exit of the combustor. This, in theory will make it possible to, for example, inject a second combustion air and burn the unburnt fuel from the first stage. If necessary, it could be injected air and fuel in the second stage to help to stabilize the secondary flame. In this way we reduce the NO_x production in the first stage and produce lower concentrations of NO_x in the lean secondary stage while having near zero unburned fuels.

A possibility that could be explored here is to use the ammonia fuel supply to inject ammonia after combustion. As it is known, NH_3 is used in the SNCR process to reduce NO_x emissions and in this way, since ammonia is already the combustion fuel, it could be used to reduce its combustion NO_x emissions. This injection could be done without using a second stage of combustion, injecting only ammonia near the exit of the combustor to reduce the emissions. However, taking the risk of undesirably increase the

NH_3 emissions, the after-combustion confinement length should be increased to give enough time for the reduction to happen. It also can be used with the second stage to reduce the emissions in there. Anyway the best approach to apply this technique should be evaluated and tested.

Regardless of all these possibilities, this burner is a laboratory scale combustion rig so the applicability of the techniques employed here should be investigated when applied to practical industrial size burners that can be used for, for example, electricity production in gas turbines.

6 References

[1] "International Energy Agency, 'Data and Statistics.'" https://www.iea.org/data-and-statistics (accessed Oct. 15, 2020).

[2] H. Kobayashi, A. Hayakawa, K. D. K. A. Somarathne, and E. C. Okafor, "Science and technology of ammonia combustion," *Proc. Combust. Inst.*, vol. 37, no. 1, pp. 109–133, 2019, doi: 10.1016/j.proci.2018.09.029.

[3] A. Valera-Medina, H. Xiao, M. Owen-Jones, W. I. F. David, and P. J. Bowen, "Ammonia for power," *Prog. Energy Combust. Sci.*, vol. 69, pp. 63–102, 2018, doi: 10.1016/j.pecs.2018.07.001.

[4] E. Baniasadi and I. Dincer, "Energy and exergy analyses of a combined ammonia-fed solid oxide fuel cell system for vehicular applications," *Int. J. Hydrogen Energy*, vol. 36, no. 17, pp. 11128–11136, 2011, doi: 10.1016/j.ijhydene.2011.04.234.

[5] S. Farhad and F. Hamdullahpur, "Conceptual design of a novel ammonia-fuelled portable solid oxide fuel cell system," *J. Power Sources*, vol. 195, no. 10, pp. 3084–3090, 2010, doi: 10.1016/j.jpowsour.2009.11.115.

[6] E. Kroch, "Ammonia - A fuel for motor buses," *Jounal Inst. Pet.*, vol. 31, pp. 213–223, 1945.

[7] D. T. Pratt, "Performance of ammonia-fired gas-turbine combustors," 1967.

[8] E. S. Starkman and G. S. Samuelsen, "Flame-propagation rates in ammonia-air combustion at high pressure," *Symp. Combust.*, vol. 11, no. 1, pp. 1037–1045, 1967.

[9] F. J. Verkamp, M. C. Hardin, and J. R. Williams, "Ammonia combustion properties and performance in gas-turbine burners," *Symp. Combust.*, vol. 11, no. 1, pp. 985–992, 1967, doi: 10.1016/S0082-0784(67)80225-X.

[10] A. J. Reiter and S. C. Kong, "Demonstration of compression-ignition engine combustion using ammonia in reducing greenhouse gas emissions," *Energy and Fuels*, vol. 22, no. 5, pp. 2963–2971, 2008, doi: 10.1021/ef800140f.

[11] A. J. Reiter and S. C. Kong, "Combustion and emissions characteristics of compression-ignition engine using dual ammonia-diesel fuel," *Fuel*, vol. 90, no. 1, pp. 87–97, 2011, doi: 10.1016/j.fuel.2010.07.055.

[12] S. S. Gill, G. S. Chatha, A. Tsolakis, S. E. Golunski, and A. P. E. York, "Assessing the effects of partially decarbonising a diesel engine by co-fuelling with dissociated ammonia," *Int. J. Hydrogen Energy*, vol. 37, no. 7, pp. 6074–6083, 2012, doi: 10.1016/j.ijhydene.2011.12.137.

[13] C. W. Gross and S. C. Kong, "Performance characteristics of a compression-ignition engine using direct-injection ammonia-DME mixtures," *Fuel*, vol. 103, pp. 1069–1079, 2013, doi: 10.1016/j.fuel.2012.08.026.

[14] K. Ryu, G. E. Zacharakis-Jutz, and S. C. Kong, "Performance characteristics of compression-ignition engine using high concentration of ammonia mixed with dimethyl ether," *Appl. Energy*, vol. 113, pp. 488–499, 2014, doi: 10.1016/j.apenergy.2013.07.065.

[15] C. S. Mørch, A. Bjerre, M. P. Gøttrup, S. C. Sorenson, and J. Schramm, "Ammonia/hydrogen mixtures in an SI-engine: Engine performance and analysis of a proposed fuel system," *Fuel*, vol. 90, no. 2, pp. 854–864, 2011, doi: 10.1016/j.fuel.2010.09.042.

[16] J. H. Lee, S. I. Lee, and O. C. Kwon, "Effects of ammonia substitution on hydrogen/air flame propagation

and emissions," *Int. J. Hydrogen Energy*, vol. 35, no. 20, pp. 11332–11341, 2010, doi: 10.1016/j.ijhydene.2010.07.104.

[17] K. Ryu, G. E. Zacharakis-Jutz, and S. C. Kong, "Performance enhancement of ammonia-fueled engine by using dissociation catalyst for hydrogen generation," *Int. J. Hydrogen Energy*, vol. 39, no. 5, pp. 2390–2398, 2014, doi: 10.1016/j.ijhydene.2013.11.098.

[18] M. Comotti and S. Frigo, "Hydrogen generation system for ammonia-hydrogen fuelled internal combustion engines," *Int. J. Hydrogen Energy*, vol. 40, no. 33, pp. 10673–10686, 2015, doi: 10.1016/j.ijhydene.2015.06.080.

[19] S. Frigo and R. Gentili, "Analysis of the behaviour of a 4-stroke Si engine fuelled with ammonia and hydrogen," *Int. J. Hydrogen Energy*, vol. 38, no. 3, pp. 1607–1615, 2013, doi: 10.1016/j.ijhydene.2012.10.114.

[20] D. H. Um, J. M. Joo, S. Lee, and O. C. Kwon, "Combustion stability limits and NOx emissions of nonpremixed ammonia-substituted hydrogen-air flames," *Int. J. Hydrogen Energy*, vol. 38, no. 34, pp. 14854–14865, 2013, doi: 10.1016/j.ijhydene.2013.08.140.

[21] A. Valera-Medina *et al.*, "Ammonia, Methane and Hydrogen for Gas Turbines," *Energy Procedia*, vol. 75, pp. 118–123, 2015, doi: 10.1016/j.egypro.2015.07.205.

[22] A. Valera-Medina *et al.*, "Ammonia–methane combustion in tangential swirl burners for gas turbine power generation," *Appl. Energy*, vol. 185, pp. 1362–1371, 2017, doi: 10.1016/j.apenergy.2016.02.073.

[23] A. Valera-Medina, D. G. Pugh, P. Marsh, G. Bulat, and P. Bowen, "Preliminary study on lean premixed combustion of ammonia-hydrogen for swirling gas turbine combustors," *Int. J. Hydrogen Energy*, vol. 42, no. 38, pp. 24495–24503, 2017, doi: 10.1016/j.ijhydene.2017.08.028.

[24] A. Valera-Medina *et al.*, "Premixed ammonia/hydrogen swirl combustion under rich fuel conditions for gas turbines operation," *Int. J. Hydrogen Energy*, vol. 44, no. 16, pp. 8615–8626, 2019, doi: 10.1016/j.ijhydene.2019.02.041.

[25] A. Hayakawa, Y. Arakawa, R. Mimoto, K. D. K. A. Somarathne, T. Kudo, and H. Kobayashi, "Experimental investigation of stabilization and emission characteristics of ammonia/air premixed flames in a swirl combustor," *Int. J. Hydrogen Energy*, vol. 42, no. 19, pp. 14010–14018, 2017, doi: 10.1016/j.ijhydene.2017.01.046.

[26] O. Kurata *et al.*, "Performances and emission characteristics of NH3-air and NH3-CH4-air combustion gas-turbine power generations," *Proc. Combust. Inst.*, vol. 36, no. 3, pp. 3351–3359, 2017, doi: 10.1016/j.proci.2016.07.088.

[27] E. C. Okafor *et al.*, "Towards the development of an efficient low-NOx ammonia combustor for a micro gas turbine," *Proc. Combust. Inst.*, vol. 37, no. 4, pp. 4597–4606, 2019, doi: 10.1016/j.proci.2018.07.083.

[28] A. A. Khateeb, T. F. Guiberti, X. Zhu, M. Younes, A. Jamal, and W. L. Roberts, "Stability limits and exhaust NO performances of ammonia-methane-air swirl flames," *Exp. Therm. Fluid Sci.*, vol. 114, no. January, p. 110058, 2020, doi: 10.1016/j.expthermflusci.2020.110058.

[29] C. Filipe Ramos, R. C. Rocha, P. M. R. Oliveira, M. Costa, and X. S. Bai, "Experimental and kinetic modelling investigation on NO, CO and NH3 emissions from NH3/CH4/air premixed flames," *Fuel*, vol. 254, no. March, p. 115693, 2019, doi: 10.1016/j.fuel.2019.115693.

[30] S. Roy, M. S. Hegde, and G. Madras, "Catalysis for NOx abatement," *Appl. Energy*, vol. 86, no. 11, pp. 2283–2297, 2009, doi: 10.1016/j.apenergy.2009.03.022.

[31] M. Radojevic, “Reduction of nitrogen oxides in flue gases,” *Environ. Pollut.*, vol. 102, no. SUPPL. 1, pp. 685–689, 1998, doi: 10.1016/S0269-7491(98)80099-7.

[32] P. Coelho and M. Costa, *Combustão*, 2nd ed. 2012.

[33] “Reotemp instruments, ‘thermocouple-types.’” https://reotemp.com/thermocouple-types/#typer (accessed Aug. 10, 2020).

[34] B. N. Taylor and C. E. Kuyatt, “Guidelines for Evaluating and Expressing the Uncertainty of NIST Measurement Results: NIST Technical Note, 1994. ISSN 17426596. doi: 10.6028/NIST.TN.1900.

[35] R. C. da Rocha, M. Costa, and X. S. Bai, “Chemical kinetic modelling of ammonia/hydrogen/air ignition, premixed flame propagation and NO emission,” *Fuel*, vol. 246, no. December 2018, pp. 24–33, 2019, doi: 10.1016/j.fuel.2019.02.102.

[36] R. C. Rocha, C. F. Ramos, M. Costa, and X. S. Bai, “Combustion of NH3/CH4/Air and NH3/H2/Air Mixtures in a Porous Burner: Experiments and Kinetic Modeling,” *Energy and Fuels*, vol. 33, no. 12, pp. 12767–12780, 2019, doi: 10.1021/acs.energyfuels.9b02948.

7 Appendices

7.1. Appendix A – Tables with the measured values

Table 7.1 - Temperature and species concentrations for flame 1. NOx in dry volume ppm, O2 in percentage (%) and temperature in ºC.

Flame 1 - x_{NH_3} = 0.7 & ϕ = 0.8														
r / z	0		5		10		15		20		25		30	
	NO_x	O_2	NO_x	O_2	NO_x	O_2	NO_x	O_2	NO_x	O_2	NO_x	O_2	NO_x	O_2
30	5409	3.7	6350.6	4.0	6322	4.4	5808	4.4						
50	5340	3.7	6326.7	4.0	5946	4.5	4713	5.0						
70	5146	3.6	6172.2	3.9	5469	4.8	3969	5.6						
90	4841	3.8	5955.0	3.9	5244	4.5	3524	5.7						
120	4420	3.9	5536.1	4.1	5118	4.7	3608	4.9						
150	3960	3.8	4950.6	4.0	4755	4.1	3809	4.4						
20	3097	4.0	3893.9	4.1	3809	4.1	3647	4.2						
250	2814	4.0	3402.8	4.2	3328	4.3	3296	4.4						
300	2768	4.0	3285.6	4.3	3247	4.4	3220	4.6						

Flame 1 - x_{NH_3} = 0.7 & ϕ = 0.8							
r / z	0	5	10	15	20	25	30
	T	T	T	T	T	T	T
30	1318	1294	1359	1444	1373	1080	813
50	1347	1343	1374	1371	1272	1117	954
70	1343	1343	1356	1337	1214	1115	1001
90	1333	1334	1347	1325	1170	1082	1019
120	1315	1321	1325	1306	1166	1088	1041
150	1268	1278	1292	1251	1172	1127	1079
200	1157	1175	1171	1154	1127	1134	1106
250	1070	1071	1066	1045	1024	1053	1043
300	987	981	979	941	914	956	944

Table 7.2 - Temperature and species concentrations for flame 2. NOx in dry volume ppm, O2 in percentage (%) and temperature in ºC.

Flame 2 - x_{NH_3} = 0.8 & ϕ = 0.8														
r / z	0		5		10		15		20		25		30	
	NO_x	O_2	NO_x	O_2	NO_x	O_2	NO_x	O_2	NO_x	O_2	NO_x	O_2	NO_x	O_2
30	3985	5.0	3777	4.9	4079	5.7	2572	6.8	288	14.1	165	8.8	249	5.8
50	3765	5.1	3762	4.7	3133	6.2	1698	8.4	416	12.5	133	10.8	122	7.7
70	3476	5.2	3614	4.6	2749	6.1	1563	8.3	605	10.7	264	10.2	137	8.7
90	3070	5.1	3461	4.5	2730	5.6	1778	7.0	737	9.4	362	9.3	174	8.9
120	2729	5.2	3060	4.6	2541	5.4	2008	5.9	1210	6.9	694	7.6	346	7.9
150	2329	5.3	2575	4.6	2217	5.4	1984	5.5	1458	6.0	1137	6.0	725	6.6
20	1855	5.3	1962	4.6	1709	5.6	1741	5.5	1528	5.5	1473	5.2	1274	5.6
250	1619	5.4	1659	4.9	1520	5.6	1681	5.4	1555	5.6	1584	5.2	1459	5.8
300	1562	5.5	1628	5.0	1461	5.9	1631	5.9	1455	6.2	1671	5.2	1526	5.5

Flame 2 - x_{NH_3} = 0.8 & ϕ = 0.8							
r / z	0	5	10	15	20	25	30
	T	T	T	T	T	T	T
30	1293	1349	1269	1336	1264	961	775
50	1303	1418	1343	1327	1227	1040	878
70	1296	1402	1313	1298	1191	1105	1016
90	1275	1295	1296	1282	1158	1125	1084
120	1244	1247	1270	1259	1187	1177	1140
150	1202	1204	1227	1217	1188	1200	1169
200	1112	1110	1129	1127	1128	1137	1144
250	1028	1022	1041	1042	1043	1041	1055
300	949	938	958	963	945	917	938

Table 7.3 - Temperature and species concentrations for flame 3. NOx in dry volume ppm, O2 in percentage (%) and temperature in ºC.

Flame 3 - x_{NH_3} = 0.9 & ϕ = 0.7														
r / z	0		5		10		15		20		25		30	
	NO_x	O_2	NO_x	O_2	NO_x	O_2	NO_x	O_2	NO_x	O_2	NO_x	O_2	NO_x	O_2
30	1652	6.5	1154	7.9	881	9.4	687	11.9	75	16.2	58	11.9	73	9.6
50	1857	6.4	1520	7.2	1109	8.9	341	14.1	72	14.4	55	12.2	72	10.4
70	1616	6.8	1616	6.8	1335	7.9	726	10.7	175	13.5	104	13.4	77	11.3
90	1430	7.1	1475	7.0	1268	7.9	1097	8.4	579	8.5	362	11.5	174	12.0
120	1141	7.2	1132	7.4	1006	7.6	1111	7.5	461	6.5	836	7.8	638	8.9
150	833	6.8	626	7.8	712	7.1	927	7.4	478	6.9	954	6.8	1009	6.9
20	660	6.5	656	7.4	569	7.1	761	7.1	719	7.5	850	6.6	939	6.6
250	542	6.5	556	6.7	455	6.8	642	6.8	560	7.5	631	6.7	533	6.9
300	450	6.5	510	6.7	347	7.0	375	7.3	427	7.4	352	7.1	294	7.4

Flame 3 - x_{NH_3} = 0.9 & ϕ = 0.7							
r / z	0	5	10	15	20	25	30
	T	T	T	T	T	T	T
30	1208	1185	1175	1197	1066	911	872
50	1195	1200	1213	1153	1036	939	867
70	1147	1161	1198	1182	1076	1048	988
90	1049	1118	1189	1197	1163	1118	1094
120	1139	1153	1157	1148	1168	1199	1171
150	1098	1104	1108	1087	1058	1208	1208
200	1016	1014	1040	1024	1050	1141	1149
250	973	982	985	983	1007	1062	1054
300	918	918	926	917	884	920	899

Table 7.4 - Temperature and species concentrations for flame 4. NOx in dry volume ppm, O2 in percentage (%) and temperature in ºC.

Flame 4 - x_{NH_3} = 0.9 & ϕ = 0.8														
r / z	0		5		10		15		20		25		30	
	NO_x	O_2	NO_x	O_2	NO_x	O_2	NO_x	O_2	NO_x	O_2	NO_x	O_2	NO_x	O_2
30	2573	4.9	2538	5.4	1775	6.3	1734	6.8	133	15.0	80	8.4	104	6.4
50	2589	4.8	2386	5.4	1431	7.3	605	11.6	106	13.2	68	9.4	84	6.9
70	2519	4.4	2788	5.2	1389	7.2	706	10.2	166	12.5	74	11.0	71	8.5
90	2205	4.5	2675	5.3	1759	5.8	1085	8.0	352	10.8	118	11.3	83	10.0
120	1856	4.6	2331	5.5	1906	5.2	1556	5.7	876	7.4	415	9.2	195	9.8
150	1651	4.3	1595	5.6	1754	5.0	1600	5.1	1287	5.3	937	6.5	582	7.0
20	1394	4.2	1287	5.3	1362	4.9	1343	4.9	1362	4.5	1197	5.6	1089	5.4
250	1294	4.3	1342	5.0	1271	4.8	1271	4.8	1263	4.7	1225	4.9	1177	5.0
300	1303	4.4	1305	5.1	1202	5.0	1257	4.9	1183	5.2	1193	5.1	1124	5.3

Flame 4 - x_{NH_3} = 0.9 & ϕ = 0.8							
r / z	0	5	10	15	20	25	30
	T	T	T	T	T	T	T
30	1281	1232	1206	1248	1206	881	798
50	1274	1267	1279	1278	1179	978	868
70	1254	1271	1269	1266	1166	1083	985
90	1243	1258	1264	1261	1162	1122	1074
120	1215	1230	1236	1242	1206	1195	1155
150	1179	1198	1199	1209	1198	1246	1217
200	1116	1124	1123	1131	1131	1200	1188
250	1044	1042	1050	1056	1051	1076	1081
300	975	972	970	971	961	930	936

Table 7.5 - Temperature and species concentrations for flame 1. NOx in dry volume ppm, O2 in percentage (%) and temperature in ºC.

Flame 5 - x_{NH_3} = 0.9 & ϕ = 0.9														
r / z	0		5		10		15		20		25		30	
	NO_x	O_2	NO_x	O_2	NO_x	O_2	NO_x	O_2	NO_x	O_2	NO_x	O_2	NO_x	O_2
30	2806	2.7	2944	3.5	2423	3.7	1091	7.0	107	13.0	93	7.2	117	5.3
50	2755	2.7	2691	3.5	1727	5.1	962	8.2	140	11.8	88	9.2	99	7.3
70	2709	2.3	2611	3.0	1790	5.1	1000	7.8	285	10.0	114	9.7	101	7.5
90	2547	2.2	2502	2.3	1789	4.7	960	7.6	578	8.2	198	9.2	127	7.4
120	2139	1.8	2166	2.2	1884	3.5	1292	5.2	814	6.2	374	7.7	204	6.4
150	1927	1.9	1869	2.2	1700	3.0	1470	3.8	1078	4.6	807	5.1	609	3.5
20	1650	1.9	1539	2.1	1473	2.9	1407	3.4	1270	3.5	1092	3.7	1118	3.0
250	1569	1.8	1455	2.7	1428	3.1	1409	3.2	1370	3.3	1235	3.6	1361	2.8
300	1591	1.8	1485	2.9	1427	3.1	1414	3.7	1395	3.7	1297	3.8	1444	3.1

Flame 5 - x_{NH_3} = 0.9 & ϕ = 0.9							
r / z	0	5	10	15	20	25	30
	T	T	T	T	T	T	T
30	1346	1299	1273	1279	1202	823	758
50	1342	1329	1352	1332	1253	1011	882
70	1323	1331	1351	1351	1296	1142	1055
90	1302	1320	1339	1348	1271	1182	1126
120	1270	1297	1314	1326	1250	1184	1159
150	1179	1198	1199	1209	1198	1246	1217
200	1164	1179	1189	1216	1197	1154	1131
250	1077	1091	1090	1123	1111	1073	1042
300	988	998	989	994	992	953	903